Strength and hydration properties of reactive MgO-activated ground granulated blastfurnace slag paste

Fei Jin[1]*, Kai Gu[2], Abir Al-Tabbaa[1]

[1] Department of Engineering, University of Cambridge, Trumpington Road, Cambridge, UK, CB2 1PZ

[2] School of Earth Sciences and Engineering, Nanjing University, Nanjing, China, 210093

* Corresponding author: Fei Jin

Email: fj232@cam.ac.uk; leonking1987@gmail.com

Tel: +44 1223 766683

Fax: +44 1223 339713

Address: Geotechnical Research Group, Engineering Department, Trumpington Road, Cambridge, UK, CB2 1PZ

Abstract: Ground granulated blastfurnace slag (GGBS) is widely used as a partial replacement for Portland cement or as the major component in the alkali-activated cement to give a clinker-free binder. In this study, reactive MgO is investigated as a potentially more practical and greener alternative as a GGBS activator. This paper focuses on of the hydration of GGBS, activated by two commercial reactive MgOs, with contents ranging from 2.5 to 20% up to 90 days. The hydration kinetics and products of MgO-GGBS blends were investigated by selective dissolution, thermogravimetric analysis, X-ray diffraction and scanning electron microscopy techniques. It was found that reactive MgO was more effective than hydrated lime in activating the GGBS based on unconfined compressive strength and the efficiency increased with the reactivity and the content of the MgO. It is hence proposed that reactive MgO has the potential to serve as an effective and economical activator for GGBS.

Key words: reactive magnesia; slag; hydrotalcite; hydration; strength; microstructure

1. Introduction

Alkali-activated ground granulated blast-furnace slag (GGBS) are sustainable alternatives to PC due to their low initial capital cost of the raw material and the saving of energy and resources, and the elimination of CO_2 emissions from chemical reactions in the kiln, leading to much lower CO_2 emissions [1]. The properties of alkali-activated slags (AAS) depend on several variables such as the GGBS composition [2], activator type and content [3,4], and curing conditions [5,6]. According to [7], the slag activation process begins with a destruction of the slag bonds (e.g., Ca-O, Mg-O, Si-O-Si, Al-O-Al and Al-O-Si) followed by the formation of a Si-Al layer all over the surface of slag grains and finally, the formation of the hydration products such as C-S-H and hydrotalcite [4]. pH is reported to be the major factor controlling the slag activation process (rather than the activating cation) with higher pH environment inducing better slag activation and higher mechanical strength [4,8,9]. Numerous research efforts have focussed on the activation of GGBS by various alkali-metal hydroxides and silicates such as NaOH, KOH or alkali salts such as waterglass and Na_2SO_4 and their mixtures [4]. However, several issues concerning the use of such strong alkalis exist, which prevent the widespread use of AAS including over-rapid setting, the difficulty of handling the caustic alkali, uneconomical efficiency and high shrinkage levels [1] in addition to potential alkali-aggregated reaction [10]. In this context, alkaline-earth hydroxides such as $Ca(OH)_2$, $Sr(OH)_2$ and $Ba(OH)_2$ have also been studied and have been found to be able to facilitate the hydration of GGBS [5,8]. Quicklime (CaO) has also been used in the activation of slags [11,12].

Recently, reactive MgO has been investigated as an activator for GGBS. Yi et al. [13] compared the strength of reactive MgO activated GGBS and $Ca(OH)_2$ activated GGBS paste at 5% and 10% activator content, and found that the former achieved ~30% higher strength than the latter after 28 days' curing at water to cement ratio (w/c) of 0.35. The use of reactive

MgO activated GGBS blends in the ground improvement application showed that 10-20% addition outperformed corresponding $Ca(OH)_2$ activated GGBS with strength values of up to 4 times higher [14]. In addition, the effect of MgO in the AAS system has been investigated by a number of researchers, either in the form of internal MgO from slag composition [15], where Mg act as an element of the glass network [16], or external MgO by additional mixing [17]. It should be noted the reactive grade (calcined at less than 1000 °C) is often selected as the external MgO added to the slag. Ben Haha et al. [15] investigated the effect of MgO content (internal) on the performance of AAS and revealed that the main hydration products are calcium silicate hydrate (C-S-H) gel and hydrotalcite-like phases (Ht), which are more voluminous than C-S-H, resulting in a less porous structure and higher strength. Thermodynamic modelling showed that up to 7% MgO content would be totally incorporated in Ht while higher content would produce brucite [15]. Gu [18] used reactive MgO to replace 40% slag with K_2CO_3 and sodium silicate as the activators and found that the strength was only slightly lower than the control although no explanation was provided regarding the role of the reactive MgO in the mix. In the work by Shen et al. [17], a commercial light-burnt dolomite (mainly contains reactive MgO and $MgCO_3$) was added in the water glass-activated slag and fly ash blends, and the results indicated that the hydration of reactive MgO decreased the shrinkage ratio of the paste, and no interaction between MgO and other components was observed in the microstructural analysis.

However, it is known that the characteristics of reactive MgO vary significantly [19], depending on their raw material, calcination conditions and the type of impurities and their content [20,21], which may affect their performance in the activation process. None of the above studies investigated the hydration kinetics of reactive MgO-GGBS paste or the effect of different types of reactive MgO on the hydration process. Furthermore, the evolution of the

hydration products requires more detailed research to elucidate the different roles that external reactive MgO and internal MgO (in the glass network) play in the mixture.

Hence this paper presents an investigation of the hydration of MgO-activated GGBS pastes using two commercially available reactive MgO samples. The hydration products were investigated by X-ray diffraction (XRD) and thermogravimetry analysis (TGA). In addition, the hydration kinetics was studied by chemical dissolution and quantification of the non-evaporable water content (NEW). Finally, scanning electron microscopy (SEM) combined with energy dispersive X-ray spectroscopy (EDS) was employed to study the microstructure and the elemental composition of the hydrated phases. Based on the experimental results, the effects of the reactivity and content of the reactive MgO on the slag activation process were discussed.

2. Materials and Methods

Two commercial reactive MgO samples, namely $MgO_{94/200}$ and $MgO_{90/200}$, obtained from Richard Baker Harrison, UK, and hydrated lime from Tarmac and Buxton Lime and Cement, UK, were used as the activators for a GGBS, obtained from Hanson, UK. Table 1 presents the composition of the MgOs, hydrated lime and the GGBS used, which shows that the major differences between those two MgOs are their CaO content ($MgO_{94/200}$ has twice the CaO content of $MgO_{90/200}$) and acetic acid reactivity [19] (smaller value indicates higher reactivity, so $MgO_{90/200}$ is more reactive). Since the chemical compositions of both MgO are similar, the large difference in their reactivity values was attributed to their calcination conditions. With the increase of burning temperature and/or burning time, the surface area and the crystal lattice decreased and the particle size increased resulting in decrease in the reactivity of MgO [22]. The BET surface area of MgO samples were determined from nitrogen adsorption-

desorption isotherms on a TriStar 3000 instrument. It is calculated from the table that the GGBS has an initial Mg/Al of ~0.78.

MgO-GGBS pastes were used in which the added MgO content ranged from 2.5% to 20% by weight of the total binder. The water to cement ratio (w/c) was set as 0.32 for all the pastes based on the standard consistence (as per [23]) of 10% $MgO_{90/200}$ and 90% GGBS paste to ensure good workability. Standard consistence is defined as the water to solid ratio which permits the Vicat plunger to penetrate to a level of 6 ± 2 mm from the bottom of the Vicat mould. Pure GGBS and hydrated lime ($Ca(OH)_2$) activated GGBS pastes were also made for comparison purpose. The nomenclature used for the mixes is X-Y, where X = M_h or M_l or C, indicating the activator used ($MgO_{90/200}$ with a higher reactivity, $MgO_{94/200}$ with a lower reactivity and $Ca(OH)_2$, respectively) and Y denotes the activator's percentage in the mix (from 2.5% to 20%) while G refers to the pure GGBS paste. The contents of the raw materials in each mix prepared are presented in Table 2.

Raw materials were mixed in a bench-top food mixer and cast into 40 mm cubic moulds. The fresh AAS paste cubes were demoulded after 24 hours and then transferred into a deionised water tank and cured for 7, 28, 56 and 90 days at a temperature of 20±1 °C. The unconfined compressive strength (UCS) of the samples, in triplicate, was then determined according to [24] at a loading rate of 2400 N/s on a CONTROLS ADVANTEST 9 strength test machine at each curing age. The crushed samples were ground and mixed with deionised water at a water to solid ratio of 1 to determine the AAS paste pore water pH according to [25], which reported that this method gave the pH values close to the directly squeezed pore water using high pressure. Eutech pH 510 meter with accuracy of 0.01 was used throughout the study.

The remaining powder and some sliced samples were stored in acetone to arrest the hydration and vacuum dried for at least 7 days prior to TG, XRD, and microstructural analyses. Once

dried, the samples were further ground to pass through a 75 μm sieve. To evaluate the slag reaction degree, duplicate 0.5 g samples were dissolved in salicyclic acid-methanol-acetone solvent and the remaining powders were filtered, dried and then ignited to 1000 °C as proposed by [26]. In this study, the commonly used Ethylenediaminetetraacetic acid **(**EDTA) method is replaced by the salicyclic acid-methanol-acetone method to determine the slag reaction degree considering the high amount of Ht formed according to [26,27]. XRD measurement was carried out on the Siemens D5000 X-ray diffractometer using a scanning range from 5 to 60 (2θ), with scanning speed of 2 s/step and resolution of 0.05 °/step to identify the hydration products formed. TGA was conducted on PerkinElmer STA6000 equipment from 40 to 1000 °C with the increasing rate of 10 °C/min. The TG curves were also used to calculate the value of NEW [6] for each sample, which is estimated from the weight loss between 50 and 800 °C after being normalised by the ignited weight of the sample. The slag reaction degree and NEW data were compared to evaluate the reaction kinetics of the MgO-GGBS blends. It was found that weight loss after 800 °C was negligible from the TGA results. SEM/EDS was performed on the JEOL 5800LV machine and roughly 30 points on each sample were picked for determination of elemental composition of the gel.

3. Results and Discussion

3.1. Unconfined compressive strength and pH development

Figure 1 shows the UCS development of the MgO-GGBS pastes together with corresponding $Ca(OH)_2$-activated GGBS pastes for comparison. For $Ca(OH)_2$-activated GGBS, the optimum activator addition was found to be 10%, which agrees well with [5]. The two types of reactive MgO samples showed different performances in activating the GGBS. Generally, the more reactive MgO ($MgO_{90/200}$) produced the higher UCS values for each curing age at the same level of MgO addition. Up to 56 days, the strength of the M_h-GGBS blends increase with the

MgO content up to 15wt%. The UCS for paste with 15% M_h addition reached approximated 40 MPa after 28 days, which was 50% higher than the corresponding $Ca(OH)_2$-GGBS paste. Further addition of MgO did not make any difference in terms of UCS. At 90 days, 10wt% MgO addition gave the highest UCS value, probably because further addition of MgO caused decrease of the GGBS content and cracks were observed to have formed due to the expansive nature of the Ht (see XRD and SEM results).

On the other hand, the UCS values of M_l-GGBS blends were only slightly higher than the inactivated GGBS up to 10wt% MgO addition. It should be noted that at 15% addition (i.e., M_l-15), there was a sharp UCS increase compared with lower additions approaching 30 MPa at 28 days and the difference between those two types of reactive MgO was reduced. Further addition to 20wt% (i.e., M_l-20) gave higher strength which was roughly the same as M_h-10. It is clear that reactive MgO activated GGBS sufficiently in terms of UCS, while the optimum addition level depended on the characteristics of the MgO.

The variation of the pH of the pore water with time and MgO content is depicted in Figure 2. Although the 7 days pH values varied significantly and seemed not to be affected by the MgO reactivity or content, all the 28 day pH values dropped to below 12 for those samples containing less than 10% MgO in the M_h-GGBS blends and less than 15% MgO in the M_l-GGBS blends. It was found that although the CaO content in M_l is twice than that in M_h, that the relative small content of this impurity did not make much difference to the whole system pH, which could be due to the relatively fast reaction between $Ca(OH)_2$ and silica in the slag to form C-S-H. The pH values of the $Ca(OH)_2$-GGBS blends were all over 12 regardless of the curing time, which explains their higher early strengths than MgO-GGBS blends with low MgO addition levels.

3.2. Slag reaction degree

The evolution of slag reaction degree with the MgO content at different curing ages is plotted in Figure 3. It shows that an increase in the curing time and MgO (both internal [15] and external) content increased the slag reaction degree. At 7 days, the slag reaction degree was extremely low for all blends and changed marginally with reactive MgO content (the high value for M_l-5 is attributed to experimental error). At 28 and 90 days, the slag reaction degree approximately increased proportionally to the reactive MgO content. In all ages, slag in M_h-GGBS blends showed higher reaction degree compared to that in M_l-GGBS blends. It should be noted that the slag reaction degree for C-10 reached 24.8% at 28 days, which is much higher than that of MG blends. The higher slag reaction degree in $Ca(OH)_2$ activated system is attributed to the higher pH as discussed above; however, it is surprising that higher strength was achieved when MgO content was over 15%. It is claimed by Ben Haha et al. [15] that higher MgO content (internal) in slag cement will increase the quantity of Ht-like phases which is more voluminous resulting in lower porosity. In order to confirm that the higher strength of MgO-GGBS blends comes from better pore filling effect of its hydration products, 10% of each activator (i.e., $Ca(OH)_2$ and M_h) was mixed with slag in different w/c.

The strength result is presented in Figure 4 in which it is obvious that in the short term (less than 28 days), $Ca(OH)_2$ activated slag showed higher strength regardless of w/c used while M_h activated slag exhibited its advantage only after 90 days. At w/c = 0.32, the UCS of the M_h-GGBS blend was approximately 50% higher as that of $Ca(OH)_2$-GGBS blend, and the discrepancy was lessened by increasing w/c. At w/c = 0.5, there was almost no difference between these two activators in terms of UCS at 90 days. It is hypothesised that at lower w/c ratio, the hydration products of MgO and GGBS were more effective by filling the pores while higher initial w/c results in larger pore volume in the cement matrix, the contribution of this pore filling effect to strength is mitigated.

3.3. Hydration Products

3.3.1. XRD

Figure 5 presents the XRD patterns for the M_h-GGBS and M_l-GGBS blends respectively with 10 and 15% MgO addition. The broad and diffuse peak at 25-35° 2θ reflects the short range order of the $CaO-Al_2O_3-MgO-SiO_2$ glass structure of the GGBS. For both reactive MgO activated GGBS paste, the characteristic peak for MgO was identified regardless of the curing time and MgO addition indicating the incomplete hydration of both reactive MgO. For M_h-GGBS blends, C-S-H can be identified as a broad peak at 2θ = ~29.5°. In addition, various peaks for tobermorite-14 Å phase were detected. Gehlenite hydrate phase at 2θ = ~25° was identified for all the mixes. The decreasing intensity of gehlenite hydrate with the increase of MgO content is consistent with the modelling results by Ben Haha et al. [3]. Newly formed peaks of Ht at 2θ = 11.7 and 22.3° were found in the M_h-10 blend after 7 days, and the peak height increased with curing time and MgO addition level indicating that more Ht formed with more MgO present and longer curing times. Calcite peaks were detected due to the impurity in the raw material and the carbonation of hydration products by exposure to the air. For M_l-GGBS blends, the abovementioned peaks for, tobermorite-like C-S-H, gehlenite hydrate and calcite were also found with relatively lower intensity suggesting lower hydration degree. In addition, Ht was only detected for the 15% M_l addition level at 28 days in the XRD pattern indicating that with the addition of the more reactive MgO, Ht is more easily formed. The XRD results agreed well with previous studies that Ht and C-S-H are the main products of alkali-activated slag when Mg is present [15,28–30]. It also suggested that Ht made a significant contribution to the strength gain as reported by [15,30]. It should be noted that in all mixes tested, no brucite was observed, suggesting that all the brucite was consumed by the reaction with GGBS, which contradicts with the modelling result by Ben Haha et al. [15].

The absence of brucite also simplified the data interpretation in the TG curves (see next section) since the decomposition temperatures of brucite and Ht overlap [31,32].

According to [33–36], the mechanism of alkali-activation includes the destruction of the prime material into low stable structural units, their interaction with coagulation structures and the creation of condensation structures. In the MgO-GGBS blends, the first steps consist of a breakdown of the slag bonds: Ca-O, Mg-O, Al-O-Al, Si-O-Si and Al-O-Si [7] and the simultaneous dissolution of MgO. Afterwards, Mg ion either reacts with Si-O or Al-O to form M-S-H or Ht in the blend and Ca reacts with Si-O and Al-O to form C-S-H and C-A-S-H. The existence of M-S-H by the reaction of MgO and silica fume at ambient temperature was confirmed in numerous papers [37–39]. However in this study, due to the low crystallinity of M-S-H [40], it is hard to be distinguished by XRD.

3.3.2. TGA

TG and first derivative of TG (DTG) signs are direct and very fast measurements of the weight loss and its rate of occurrence during analysis, by which different materials are identified based on their thermal characteristics [41]. The DTG curves of M_h-GGBS and M_l-GGBS blends with varying MgO addition are shown in Figure 6. From the DTG curves, three major humps involving several tiny peaks were observed as described below:

1. At temperatures up to 250 °C, this involves the dehydration of C-S-H, and possibly M-S-H [39,42]. The small shoulder at ~80-130 °C could be attributed to AFm, gehlenite hydrate [41,43] or Ht [44].
2. The temperature range of 300 to 550 °C includes mainly the decomposition of Ht since brucite was found to be totally consumed by the reaction with slag from the XRD analysis. In addition, the tiny peak at around 530 °C was attributed to the loss of coordinated water in M-S-H [39,45].

3. The temperature range of 550 to 800 °C is the decomposition range of various carbonate-containing phases including magnesium carbonate, calcite [46] and Ht [47], originating from the raw material and the carbonation due to exposure to the air.

Although several authors [48,49] tried to quantify each hydration phase by thermal analysis, it is claimed that the quantification of the amount of each phase is not possible since there are too many overlaps in each temperature range [30]. Therefore the weight loss is divided into three main stages without differentiation between the phases. The first weight loss between 50 and 250 °C, in this study is denoted as Δm_1 and the second hump at 250-550 °C denoted as Δm_2. In addition, the NEW was calculated by the weight loss between 50 and 800 °C. Herein all the weight losses were divided by the final ignited mass.

Table 3 lists the evolution of Δm_1, Δm_2 and NEW with the increase of reactive MgO addition and curing time. There is a clear trend of an increase of all three variables for the MgO-GGBS blends with the increase of MgO content as well as the curing time, which is attributed to the higher hydration degree thus more hydration products formed. Generally, with the same amount of reactive MgO addition, M_h-GGBS blends give higher values for all of the three variables. The TG data agreed well with the UCS results considering that an increase in the hydration products causes strength gain due to filling of pores occupied by water previously.

Non-evaporable water content is often used as a measurement of the hydration extent of plain Portland-cement pastes [50] and also blended cements with slags [3,6]. The approximate linear relationship between NEW and slag reaction degree is presented in Figure 7. The imperfect fitting is attributed to the varying composition and stoichiometry of the hydration products. The correlation between NEW and UCS is depicted in Figure 8, which shows an approximately linear relationship in the short term (7 and 28 days, in this study), which is in

agreement with [3,51]. However, at 90 days, the linear relationship is not satisfactory due to (a) the evolution of the hydration products and the change of the stoichiometry, e.g., the change of the incorporated water content in the C-S-H and Ht structure [52]; and (b) the formation of the cracks resulted from expansion of the hydration products, i.e., although the hydration is still progressing, the strength gain stops due to cracking in the cement matrix.

3.3.3. Microstructural and elemental analysis

SEM images of M_h-GGBS blends with 5, 10, and 15% MgO additions are shown in Figure 9. At 5% addition, the irregular slag particles were loosely stacked, which explains its low strength. Significant changes are observed in M_h-10 and M_h-15 blends, showing a much denser microstructure with irregular slag particles connected by gels. The C-S-H aggregates were distributed on the surface (Figure 9 (d) and (f)). In addition, small cracks were visible for both M_h-10 and M_h-15 blends (Figure 9 (d), (e) and (f)) due to the expansive nature of hydration products and the low water to cement ratio used in this study. Fibrous Ht was detected in M_h-15 blend growing on the C-S-H gels (Figure 9 (f)), which agrees with the XRD results. According to the modelling of [15], Ht phases are more voluminous than C-S-H gels, resulting in a matrix with lower porosity in an adequate quantity; however, it is found that when too much reactive MgO is present in the blend, the over-expansion causes volume instability and may be detrimental to the strength. This is probably the reason why after 28 days, there is almost no strength gain for MgO_h-GGBS blends at over 10% reactive MgO addition (Figure 1(a)).

To determine the elemental compositions of the hydration products, EDS were performed on resin-impregnated polished samples. Roughly 30 points on the gel were picked up for each sample at a magnification of 2500. Figure 10 plots the Mg/Ca vs. Al/Ca ratios of the gels in the M_h-GGBS blends hydrated for 7 and 28 days. Extrapolating the straight line to Mg/Ca = 0 gives a positive number, indicating that the C-S-H gel also contains a proportion of

aluminium either in solid solution within the C-S-H structure or in an AFm form finely intermixed with it [29]. There is a linear relationship between the two ratios with the points lying on a line with Mg/Al ratio of 1.08 for blends with 5% reactive MgO content regardless of the curing time. With the increase of reactive MgO content, it is clear that the data points locate mostly above the fitted line indicating that the Mg/Al ratio increases. Due to the large variation of the data, it is not possible to generate a linear relationship between reactive MgO content and the Mg/Al ratio, which revealed the heterogeneity of the Ht composition, giving support for inconsistent changes of the NEW data with curing time as mentioned above. It should be noted that the result is contrary to the findings regarding the effect of internal MgO on the Mg/Al ratio according to [15], who found that the Mg/Al ratio barely changed with increased MgO content in the slag composition.

3.4. Discussion

The hydration chemistry that involves MgO and other cementitious materials was summarised by Bakharev [53]. In PC paste, brucite is the most favoured product, while in the presence of fly ash, silica fume and/or slag, brucite is usually accompanied with hydrotalcite and M-S-H gel [53]. In alkali-activated slag paste, Ben Haha et al. [15] revealed that the main hydration products are C-S-H gel and Ht, where a higher content of MgO in slag composition produced more Ht. However, those studies only investigated dead burned MgO from PC or MgO in the glass network from the slag composition instead of reactive MgO as an additive in the mix.

Recently, the hydration between reactive MgO and conventional cement additives were studied extensively. In the reactive MgO and silica fume blend, it was found that M-S-H was the major hydration product [37,39]. Vandeperre et al. [54] studied the microstructure of the reactive MgO and pulverized fly ash (PFA) blends and observed brucite and a very small

quantity of hydrotalcite from by XRD, which was consistent with results in [55], who reported the formation of Ht on hydrating mixtures of alumina with reactive MgO. Combining the hydration mechanisms of conventional alkali-activated slag (i.e., glass network of CaO-MgO-Al_2O_3-SiO_2) [33–36], the hydration mechanisms of reactive MgO-GGBS can be proposed.

In contact of water, MgO dissolves as follows [56]:

$$MgO + H_2O \rightarrow Mg^{2+} + 2OH^- \quad (1)$$

The dissolution of MgO provides an alkaline environment followed by the breakdown of the covalent bonds (Si-O-Si and Al-O-Si) in GGBS particles [57]. Impermeable coatings of aluminosilicates deposit on the surface of the slag grains within a few minutes of exposure to water, hindering further hydration reaction [4]. If the pH is not high enough, there will not be sufficient OH^- to break the Si-O and Al-O bonds for the formation of the hydration products. Song et al. [4] claimed that the pH should be over 11.5 to initiate the activation process, while in another study, the value is reported as 12 [58]. The results in this study seem to confirm the latter value and also demonstrated that 10-15% reactive is able to maintain the pH value above 12 to activate GGBS effectively.

Afterwards, Mg^{2+} either reacts with Si-O or Al-O to form M-S-H or Ht. From the XRD results, it was found that no brucite was left even with up to 20% $MgO_{90/200}$. Therefore, the overall hydration reaction of reactive MgO and GGBS blends was summarised as:

$$CaO\text{-}MgO\text{-}Al_2O_3\text{-}SiO_2 \text{ (slag)} + MgO + H_2O \rightarrow C\text{-}S\text{-}H + M\text{-}S\text{-}H + M\text{-}A\text{-}H \text{ (Ht)} + C\text{-}A\text{-}S\text{-}H \quad (2)$$

The formed Ht has a significant effect on the mechanical performance of reactive MgO-GGBS blends since it occupies more space than C-S-H resulting in less porosity compared to

the corresponding $Ca(OH)_2$-GGBS blends. Preliminary study showed that by increasing the $MgO_{90/200}$ content to 50% or by using a highly reactive MgO (reactivity value = 10 s, at 20%), brucite was also detected in the blends since in that case, the consumption rate of Mg^{2+} by slag was lower than the dissolution rate of MgO. Consequently, the pore water will soon be supersaturated by Mg^{2+} and OH^- and $Mg(OH)_2$ nucleation and growth set immediately:

$$Mg^{2+} + 2OH^- \rightarrow Mg(OH)_2\ (s) \quad (3)$$

In this study, up to 20% $MgO_{90/200}$ did not produce any brucite since the dissolved Mg^{2+} was soon consumed by the slag and was not able to achieve the supersaturation state.

The composition of the Ht in various cement systems has been studied by many researchers. For the cases of MgO contained in slag composition, it is claimed that the slag (initial Mg/Al=1.51) hydration produce the same form of Ht (Mg/Al ≈ 2.30-2.55) no matter what system it has been put into: unactivated, PC blend or hydrated lime-activated [29]. Contrary to that, Ben Haha et al. [30] found Mg/Al ratio of the hydration products were 1.24, 1.38 and 2.02 when the initial Mg/Al in the raw material (by increasing Al content) were 0.49, 0.60 and 1.29, respectively, while MgO content has no effect on the Mg/Al ratio [15]. Yi et al. [13] investigated the $Ca(OH)_2$ activated slag (initial Mg/Al = 0.86) and found the Mg/Al ratio in the hydration products was ~1.1. On the other hand, when reactive MgO was added, Yi et al. [13] reported a Mg/Al ratio of ~2.0 when reactive MgO content was 10% and 20% in the MgO-GGBS mixture although the variation of the data was relatively large. In this study, note that the initial Mg/Al is ~0.78 in the slag used here. It is found that 5% of reactive MgO addition generates the Ht with Mg/Al ratio of ~1.1, which is consistent with Yi et al. [13] and Ben Haha et al. [30]. The Mg/Al ratio increased with the increase of reactive MgO content in the mix; however, this ratio varies in a wide range indicating the heterogeneous composition of the Ht formed when using reactive MgO compared to that formed by internal MgO.

Therefore, we conclude that the Mg/Al of the Ht is highly dependent on the initial slag composition and the content of reactive MgO added. In the absence of added reactive MgO, when the initial Mg/Al (Mg from slag) is 0.49-0.86, the Mg/Al of Ht was found to be 1.1-1.38, while increasing the initial Mg/Al to 1.29-1.51 generates Ht with a Mg/Al of 2.02-2.55. When reactive MgO was added, the quick dissolution of reactive MgO generated more available Mg^{2+} in the short term; however, 5% addition did not change Mg/Al of Ht much, which could be due to the combination of Mg in other phases such as M-S-H [37,39]. More than 10% reactive MgO produced Ht with a highly heterogeneous nature showing a wide range of Mg/Al ratio.

4. Conclusions

By comparing the UCS, pH values and porosity of MgO-GGBS blends, using two different reactive MgOs, and also with $Ca(OH)_2$-GGBS blends and studying their hydration products by means of XRD, TGA and SEM/EDS, reactive MgO is found to activate GGBS effectively. The following conclusions can be drawn:

1. The reactivity of MgO affects the performance of MgO-GGBS blends, such that the more reactive MgO gives higher UCS values and more hydration products in the same curing time.
2. The pH is found to be the major controlling factor in the activation process, which is affected by the reactivity and content of reactive MgO.
3. Although reactive MgO dissolves less slag in the same curing time compared to $Ca(OH)_2$ due to lower pH, it is found that higher strength can be achieved at the low w/c, which is attributed to better pore filling capacity of the hydration products.
4. The main hydration products are hydrotalcite-like phases (Ht) and calcium silicate hydrate (C-S-H), with the content increase with the increase of MgO addition and curing time.

5. The non-evaporable water (NEW) content is found to be a useful indicator of the extent of hydration and there is an approximately linear relationship between NEW and slag reaction degree. Besides, UCS is also positively correlated with NEW in the short term until excess hydration products cause microcracks in the matrix.
6. The composition of Ht depends on the reactive MgO content. GGBS activated by 5% reactive MgO produces Ht with Mg/Al ratio of ~1.1 while more than 10% reactive MgO addition generates heterogeneous Ht with Mg/Al ratio spreading in a wide range above 1.1.

Acknowledgements

The authors are grateful to Cambridge Trust and China Scholarship Council (CSC) for their financial help of the PhD studentship for the first author.

References

[1] Yang K-H, Cho A-R, Song J-K, Nam S-H. Hydration products and strength development of calcium hydroxide-based alkali-activated slag mortars. Constr Build Mater 2012;29:410–9.

[2] Beushausen H, Alexander M, Ballim Y. Early-age properties, strength development and heat of hydration of concrete containing various South African slags at different replacement ratios. Constr Build Mater 2012;29:533–40.

[3] Haha MB, Saout GL, Winnefeld F, Lothenbach B. Influence of activator type on hydration kinetics, hydrate assemblage and microstructural development of alkali activated blast-furnace slags. Cem Concr Res 2011;41:301–10.

[4] Song S, Sohn D, Jennings H. Hydration of alkali-activated ground granulated blast furnace slag. J Mater Sci 2000;35:249 – 257.

[5] Yang K-H, Sim J-I, Nam S-H. Enhancement of reactivity of calcium hydroxide-activated slag mortars by the addition of barium hydroxide. Constr Build Mater 2010;24:241–51.

[6] Escalante J. Reactivity of blast-furnace slag in Portland cement blends hydrated under different conditions. Cem Concr Res 2001;31:1403–9.

[7] Krizan D, Zivanovic B. Effects of dosage and modulus of water glass on early hydration of alkali–slag cements. Cem Concr Res 2002;32:1181–8.

[8] Roy A, Schilling P, Eaton H. Activation of ground blast furnace slag by alkali metal and alkaline earth hydroxides. J Am Ceram Soc 1992;75:3233–40.

[9] Wang S, Scrivener K, Pratt P. Factors affecting the strength of alkali-activated slag. Cem Concr Res 1994;24:1033–43.

[10] Shi C, Krivenko PV, Roy DM. Alkali-Activated Cements and Concretes. Taylor & Francis, 2006.

[11] Obuzor GN, Kinuthia JM, Robinson RB. Enhancing the durability of flooded low-capacity soils by utilizing lime-activated ground granulated blastfurnace slag (GGBS). Eng Geol 2011;123:179–86.

[12] Obuzor GN, Kinuthia JM, Robinson RB. Utilisation of lime activated GGBS to reduce the deleterious effect of flooding on stabilised road structural materials: A laboratory simulation. Eng Geol 2011;122:334–8.

[13] Yi Y, Liska M, Al-Tabbaa A. Properties and microstructure of GGBS-MgO pastes. Adv Cem Res 2014;26: 114-122.

[14] Yi Y, Liska M, Al-Tabbaa A. Initial investigation into the use of GGBS-MgO in soil stabilisation. Proc 4th Int. Conf. Grouting Deep Mix., New Orleans: 2012, p. 444–53.

[15] Ben Haha M, Lothenbach B, Saout G Le, Winnefeld F. Influence of slag chemistry on the hydration of alkali-activated blast-furnace slag—Part I: Effect of MgO. Cem Concr Res 2011;41:955–63.

[16] Hewlett P. Lea's Chemistry of Cement and Concrete. Elsevier Science & Technology Books, 2004.

[17] Shen W, Wang Y, Zhang T, Zhou M, Li J, Cui X. Magnesia modification of alkali-activated slag fly ash cement. J Wuhan Univ Technol Sci Ed 2011;26:121–5.

[18] Gu J. Hydration mechanism, properties and application of alkali-slag cement. Cem Concr Prod (in Chinese) 1991;5:8–11.

[19] Shand M. The Chemistry and Technology of Magnesia. Hoboken, New Jersey: John Wiley & Sons, Ltd., 2006.

[20] Birchal V, Rocha S, Ciminelli V. The effect of magnesite calcination conditions on magnesia hydration. Miner Eng 2000;13:1629–33.

[21] Mo L, Deng M, Tang M. Effects of calcination condition on expansion property of MgO-type expansive agent used in cement-based materials. Cem Concr Res 2010;40:437–46.

[22] Jin F, Al-Tabbaa A. Characterisation of different commercial reactive magnesia. Adv Cem Res 2014;26:101–13.

[23] British Standard EN 196-3. Methods of testing cement part 3:Determination of setting times and soundness. 2005.

[24] British Standard EN 196-1. Methods of testing cement part 1: Determination of strength. 2005.

[25] Göran Bäckblom. R&D on low-pH cement for a geological repository. 2004.

[26] Luke K, Glasser FP. Selective dissolution of hydrated blast furnace slag cements. Cem Concr Res 1987;17:273–82.

[27] Gruskovnjak A, Lothenbach B, Winnefeld F, Münch B, Figi R, Ko S-C, et al. Quantification of hydration phases in supersulfated cements: review and new approaches. Adv Cem Res 2011;23:265–75.

[28] Wang S, Scrivener K. Hydration products of alkali activated slag cement. Cem Concr Res 1995;25:561–71.

[29] Richardson J, Biernacki J. Stoichiometry of slag hydration with calcium hydroxide. J Am Ceram Soc 2002;85:947–53.

[30] Ben Haha M, Lothenbach B, Le Saout G, Winnefeld F. Influence of slag chemistry on the hydration of alkali-activated blast-furnace slag — Part II: Effect of Al2O3. Cem Concr Res 2012;42:74–83.

[31] Aphane ME, van der Merwe EM, Strydom CA. Influence of hydration time on the hydration of MgO in water and in a magnesium acetate solution. J Therm Anal Calorim 2009;96:987–92.

[32] Constantino V, Pinnavaia T. Basic Properties of Mg2+1-xAl3+x Layered Double Hydroxides Intercalated by Carbonate, Hydroxide, Chloride, and Sulfate Anions. Inorg Chem 1995;34:883–92.

[33] Pacheco-Torgal F, Castro-Gomes J, Jalali S. Alkali-activated binders: A review. Part 2. About materials and binders manufacture. Constr Build Mater 2008;22:1315–22.

[34] Yip C, Lukey G, van Deventer J. The coexistence of geopolymeric gel and calcium silicate hydrate at the early stage of alkaline activation. Cem Concr Res 2005;35:1688–97.

[35] Provis J, Lukey G, van Deventer J. Do geopolymers actually contain nanocrystalline zeolites? A reexamination of existing results. Chem Mater 2005;17:3075–85.

[36] Provis J, Duxson P, Van Deventer J, Lukey G. The Role of Mathematical Modelling and Gel Chemistry in Advancing Geopolymer Technology. Chem Eng Res Des 2005;83:853–60.

[37] Zhang T, Cheeseman CR, Vandeperre LJ. Development of low pH cement systems forming magnesium silicate hydrate (MSH). Cem Concr Res 2011;41:439–42.

[38] Wei J, Chen Y, Li Y. Reaction mechanism between MgO and microsilica at room temperature. J Wuhan Univ Technol Mater Sci Ed 2006;21:88–91.

[39] Jin F, Al-Tabbaa A. Thermogravimetric study on the hydration of reactive MgO and silica mxiture at room temperature. Thermochim Acta 2013;566:162–8.

[40] Brew D, Glasser F. Synthesis and characterisation of magnesium silicate hydrate gels. Cem Concr Res 2005;35:85–98.

[41] Ramachandran VS, Paroli RM, Beaudoin JJ, Delgado AH. Handbook of Thermal Analysis of Construction Materials. Ontario, Canada: William Andrew Publishing, 2002.

[42] Dweck J, Buchler P, Coelho A, Cartledge F. Hydration of a Portland cement blended with calcium carbonate. Thermochim Acta 2000;346:105–13.

[43] Sha W. Differential scanning calorimetry study of the hydration products in Portland cement pastes with metakaolin replacement. Proc Int Conf Adv Build Technol 2002;1,2:881–8.

[44] Palmer S, Frost R, Vágvölgyi V, Kristóf J, Horváth E. Mechanism for hydrotalcite decomposition: A controlled rate thermal analysis study. J Colloid Interface Sci 2008;318:302–8.

[45] Tartaglione G, Tabuani D, Camino G. Thermal and morphological characterisation of organically modified sepiolite. Microporous Mesoporous Mater 2008;107:161–8.

[46] Dweck J, Ferreira da Silva P, Büchler P, Cartledge F. Study by thermogravimetry of the evolution of ettringite phase during type II Portland cement hydration. J Therm Anal Calorim 2002;69:179–86.

[47] Parashar P, Sharma V, Agarwal DD, Richhariya N. Rapid synthesis of hydrotalcite with high antacid activity. Mater Lett 2012;74:93–5.

[48] Cabrera J. The effect of temperature on the hydration rate and stability of the hydration phases of metakaolin – lime – water systems. Cem Concr Res 2002;32:133–8.

[49] Cabrera J, Rojas M. Mechanism of hydration of the metakaolin lime water system. Cem Concr Res 2001;31:177–82.

[50] Escalante-Garcia JI. Nonevaporable water from neat OPC and replacement materials in composite cements hydrated at different temperatures. Cem Concr Res 2003;33:1883–8.

[51] Gruyaert E, Robeyst N, De Belie N. Study of the hydration of Portland cement blended with blast-furnace slag by calorimetry and thermogravimetry. J Therm Anal Calorim 2010;102:941–51.

[52] García Giménez R, Rodríguez O, Vigil de la Villa R, Frías M. Changes to the Triaxial Composition of the Hydrated Phases (CaO/Al2O3/SiO2) in the Metakaolin/Lime System. J Am Ceram Soc 2012;95:1118–22.

[53] Bakharev T. Durability of geopolymer materials in sodium and magnesium sulfate solutions. Cem Concr Res 2005;35:1233–46.

[54] Vandeperre LJ, Liska M, Al-Tabbaa A. Microstructures of reactive magnesia cement blends. Cem Concr Compos 2008;30:706–14.

[55] Ghanbari Ahari K, Sharp JH, Lee WE. Hydration of refractory oxides in castable bond systems--I: alumina, magnesia, and alumina-magnesia mixtures. J Eur Ceram Soc 2002;22:495–503.

[56] Fruhwirth O, Herzog G, Hollerer I, Rachetti A. Dissolution and hydration kinetics of MgO. Surf Technol 1985;24:301–17.

[57] Li C, Sun H, Li L. A review: The comparison between alkali-activated slag (Si+Ca) and metakaolin (Si+Al) cements. Cem Concr Res 2010;40:1341–9.

[58] Zhou J, Guang Y, van Breugel K. Hydration of Portland cement blended with blast furnace slag at early age. In: Marchand J, Bissonnette B., Gagne R., Jolin M., Paradis F., editors. Second Int. Symp. Adv. Concr. through Sci. Eng., Quebec, Canada, 2006.

Figure 1 UCS development with time (a) M_h-GGBS blends (b) M_l-GGBS blends

Figure 2 Variation of pH with curing time (a) M_h-GGBS blends (b) M_l-GGBS blends

Figure 3 Slag reaction degrees with different MgO content

Figure 4 Effect of W/C on the strength of M_h-GGBS and C-10 blends

Figure 5 XRD patterns for (a) M_h-10 and M_h-15 and (b) M_l-10 and M_l-15 blends cured for 7 and 28days. Ht: hydrotalcite-like phases; C: tobermorite-like C-S-H; G: gelenite hydrate; CC: calcite; M: MgO

Figure 6 DTG curves for (a) M_h-GGBS blends and (b) M_l-GGBS blends cured for 28days

Figure 7 Relationship between slag reaction degree and NEW

Figure 8 Relationship between UCS of MgO-GGBS blends and NEW

Figure 9 SEM pictures for M_h-GGBS blends at 28 days (a)(b) 5% MgO; (c)(d) 10% MgO; (e)(f) 15% MgO

Figure 10 Mg/Ca against Al/Ca atom ratio plot for M_h-GGBS blends

Table

Table 1 Physical properties and chemical compositions of MgO, $Ca(OH)_2$ and GGBS, from suppliers' datasheets

Label		$MgO_{94/200}$	$MgO_{90/200}$	$Ca(OH)_2$	GGBS
Chemical composition (wt%)	MgO	94	93.2	-	8
	CaO	2	0.9	-	40
	$Ca(OH)_2$	-	-	96.9	-
	$CaCO_3$	-	-	1.4	-
	SiO_2	1	0.9	-	37
	Fe_2O_3	0.7	0.5	-	-
	Al_2O_3	-	0.22	-	13
	$Mg(OH)_2$	-	-	0.5	0.4
	Na_2O	-	-	-	0.3
	K_2O	-	-	-	0.6
	SO_3	-	-	0.02	2.5
Reactivity* (s)		976.0	100.4	-	-
Specific surface area (m^2/kg)		4400	9005	1529	493

* measured in the laboratory using the acetic acid test [19]

Table 2 Mix design of MgO-GGBS pastes

Paste Nomenclature	Weight percentage /%			
	$MgO_{90/200}$	$MgO_{94/200}$	$Ca(OH)_2$	GGBS
G	0			100
M_h -2.5	2.5			97.5
M_h -5	5			95
M_h -7.5	7.5			92.5
M_h -10	10			90
M_h -15	15			85
M_h -20	20			80
M_l -2.5		2.5		97.5
M_l -5		5		95
M_l -7.5		7.5		92.5
M_l -10		10		90
M_l -15		15		85
M_l -20		20		80
C-5			5	95
C-10			10	90
C-15			15	85

Table 3 Calculated weight loss from TG curves

Paste Denotation	Weight percentage /%								
	7d			28d			90d		
	Δm_1	Δm_2	NEW	Δm_1	Δm_2	NEW	Δm_1	Δm_2	NEW
G	1.47	1.23	3.35	1.75	1.79	4.40	3.03	1.90	6.84
M_h -2.5	1.76	1.56	4.36	2.60	1.94	6.00	3.27	2.54	8.07
M_h -5	2.29	2.02	5.43	2.86	2.14	6.00	3.92	3.00	9.01
M_h -7.5	2.40	2.06	5.60	3.37	2.96	7.77	4.39	3.25	10.05
M_h -10	3.20	3.04	8.18	5.14	3.83	11.21	5.11	4.19	11.00
M_h -15	3.26	3.86	9.30	6.92	4.64	13.48	6.73	5.26	14.44
M_h -20	4.29	4.18	10.57	6.41	5.30	14.08	7.07	6.35	16.38
M_l -2.5	1.65	1.58	3.90	1.99	1.68	4.65	3.10	2.19	7.53
M_l -5	1.87	1.53	4.44	2.60	1.97	5.77	3.12	2.28	8.04
M_l -7.5	1.43	1.20	3.47	2.62	1.95	5.90	3.84	2.91	9.24
M_l -10	1.61	1.39	3.98	2.97	2.16	6.54	4.10	2.91	9.24
M_l -15	1.62	1.87	5.38	6.00	2.95	10.26	5.90	4.29	13.38
M_l -20	1.78	1.80	5.31	5.99	3.10	10.53	6.26	4.39	13.35

Figure
Click here to download high resolution image

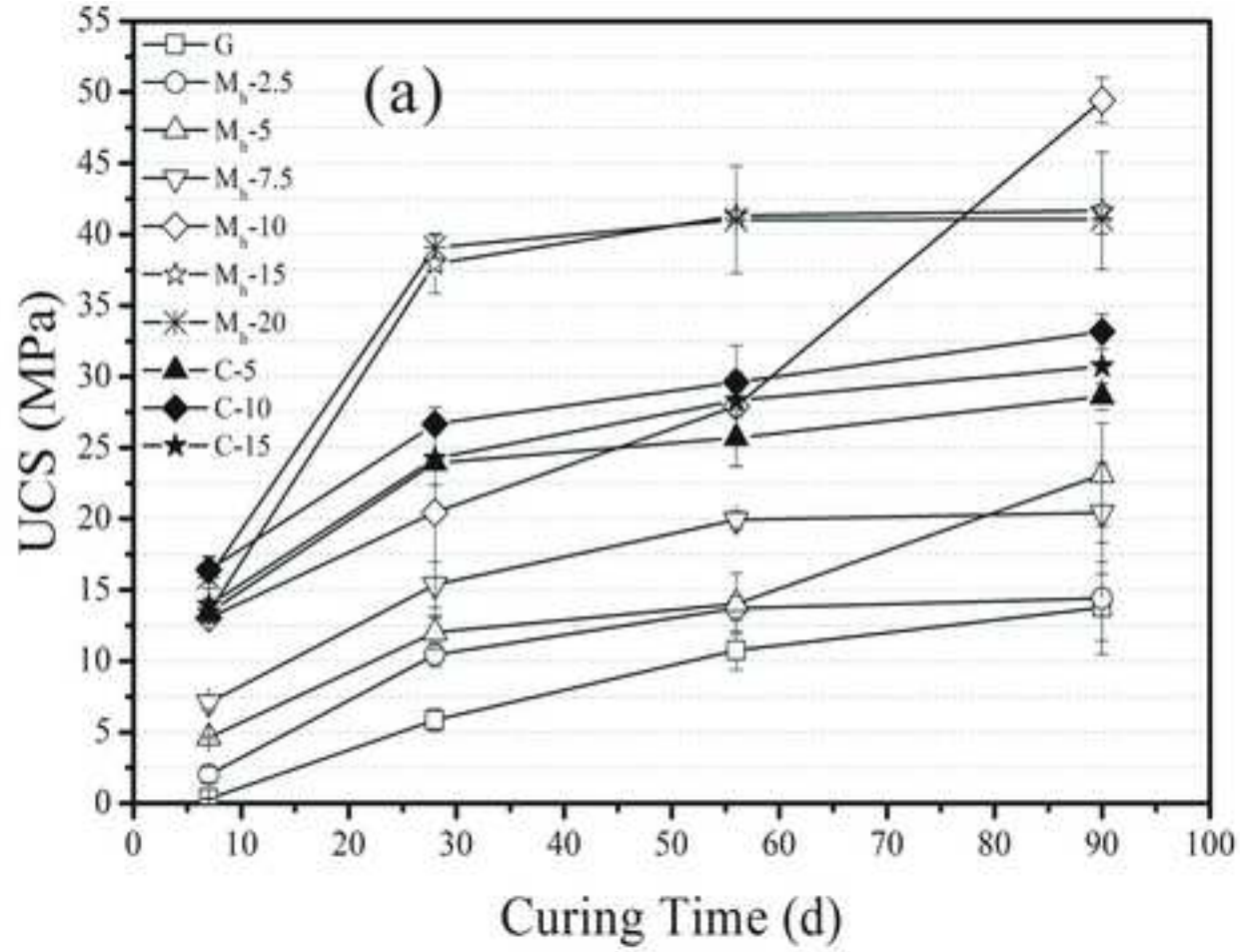

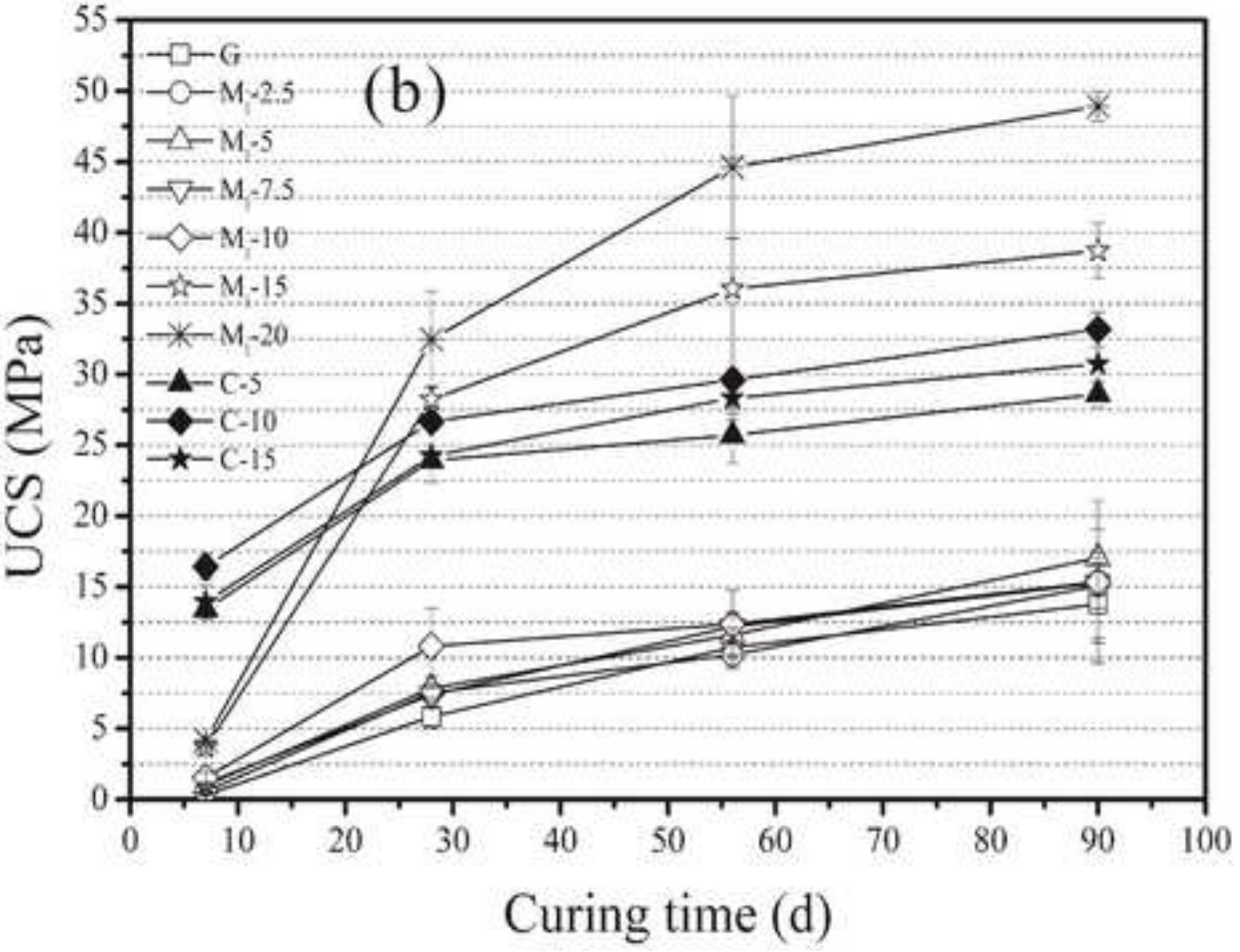

Figure

Click here to download high resolution image

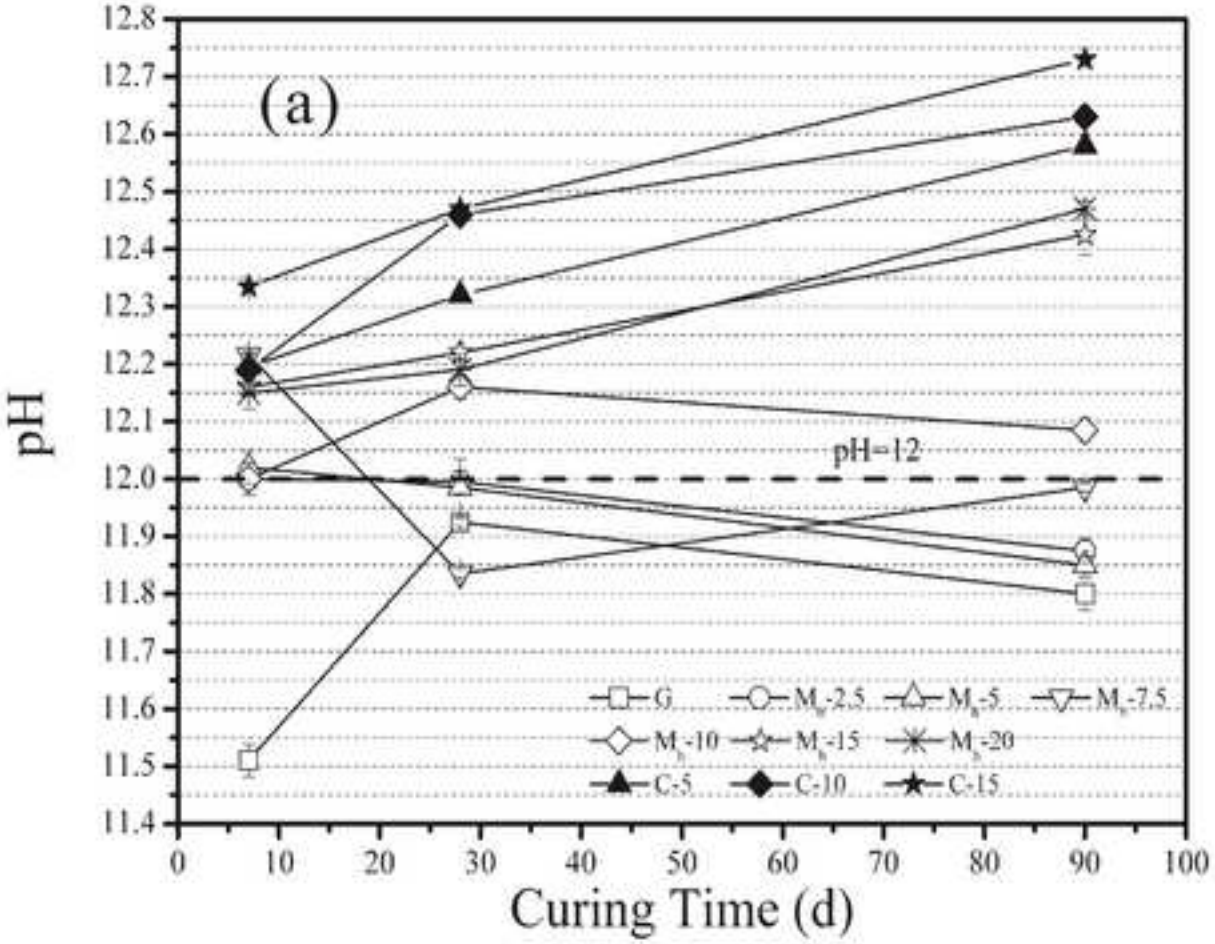

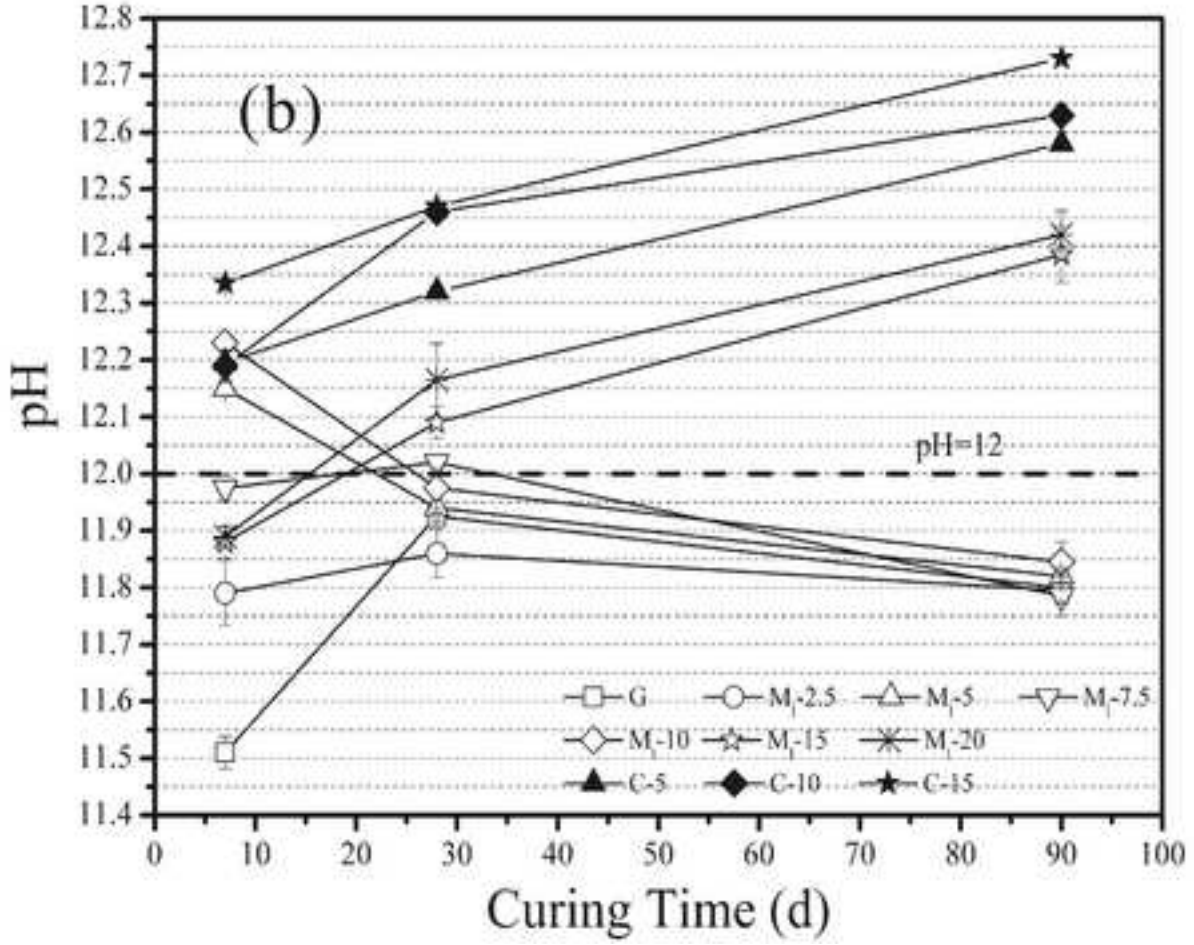

Figure

Click here to download high resolution image

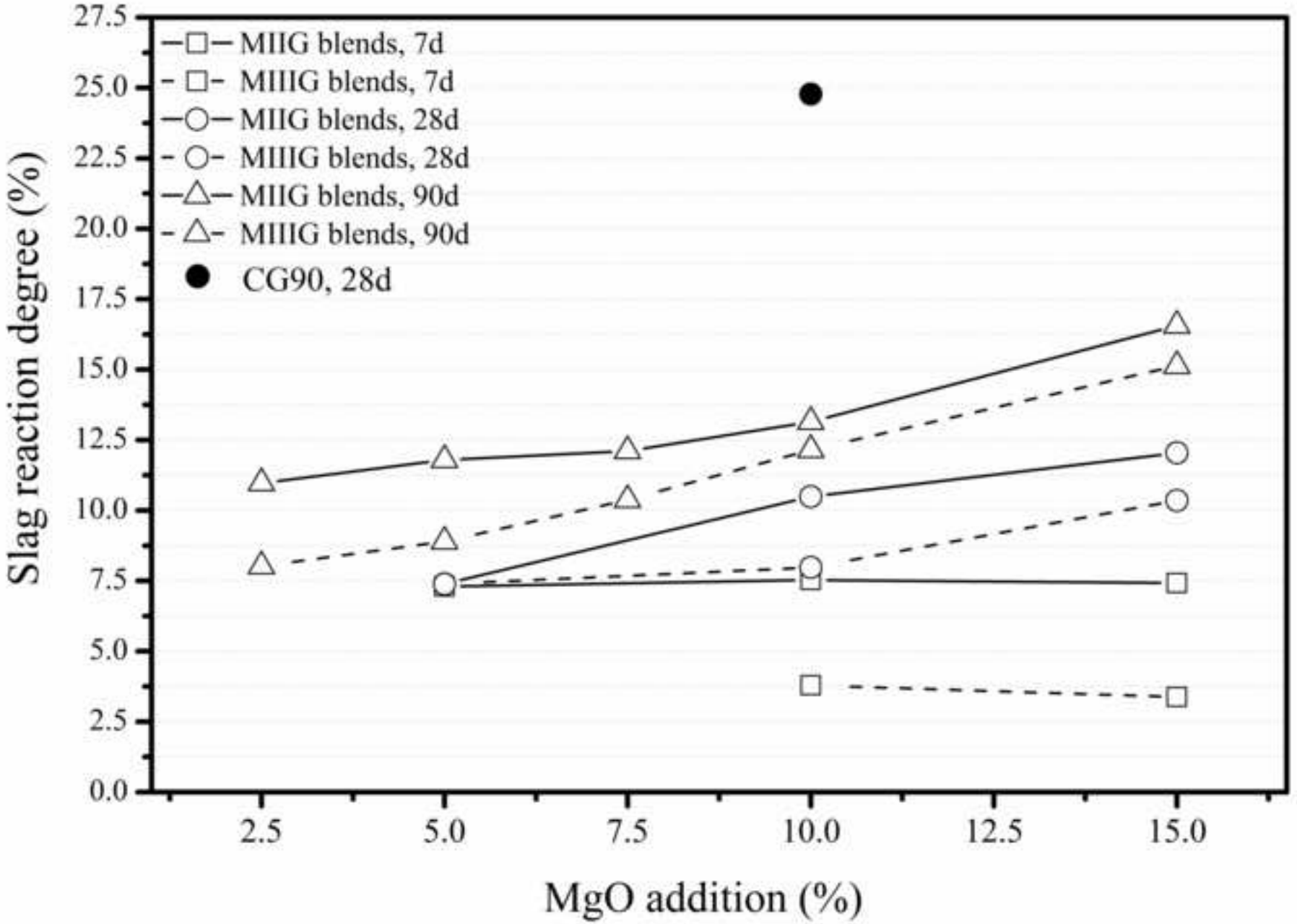

Figure

Click here to download high resolution image

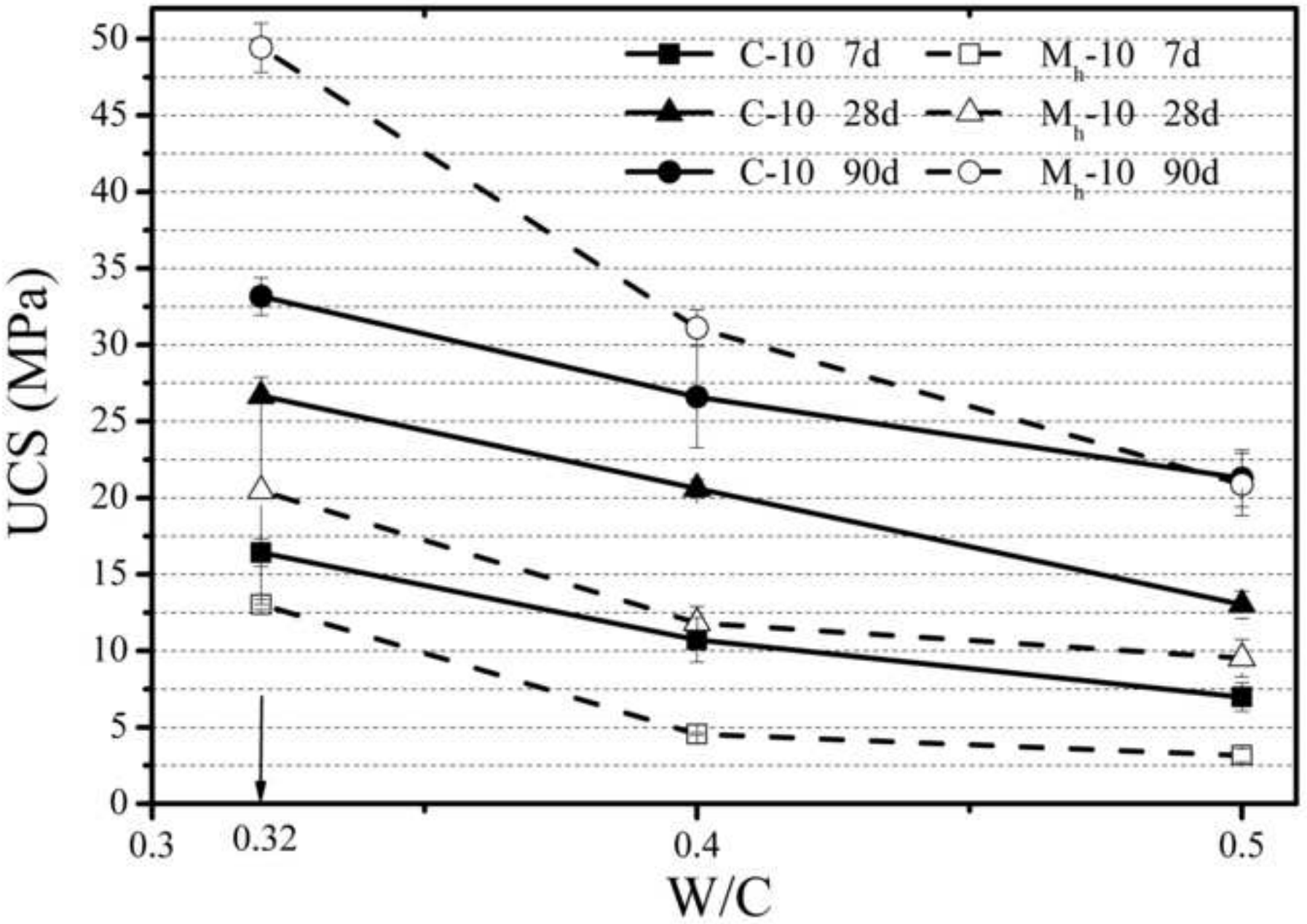

Figure
Click here to download high resolution image

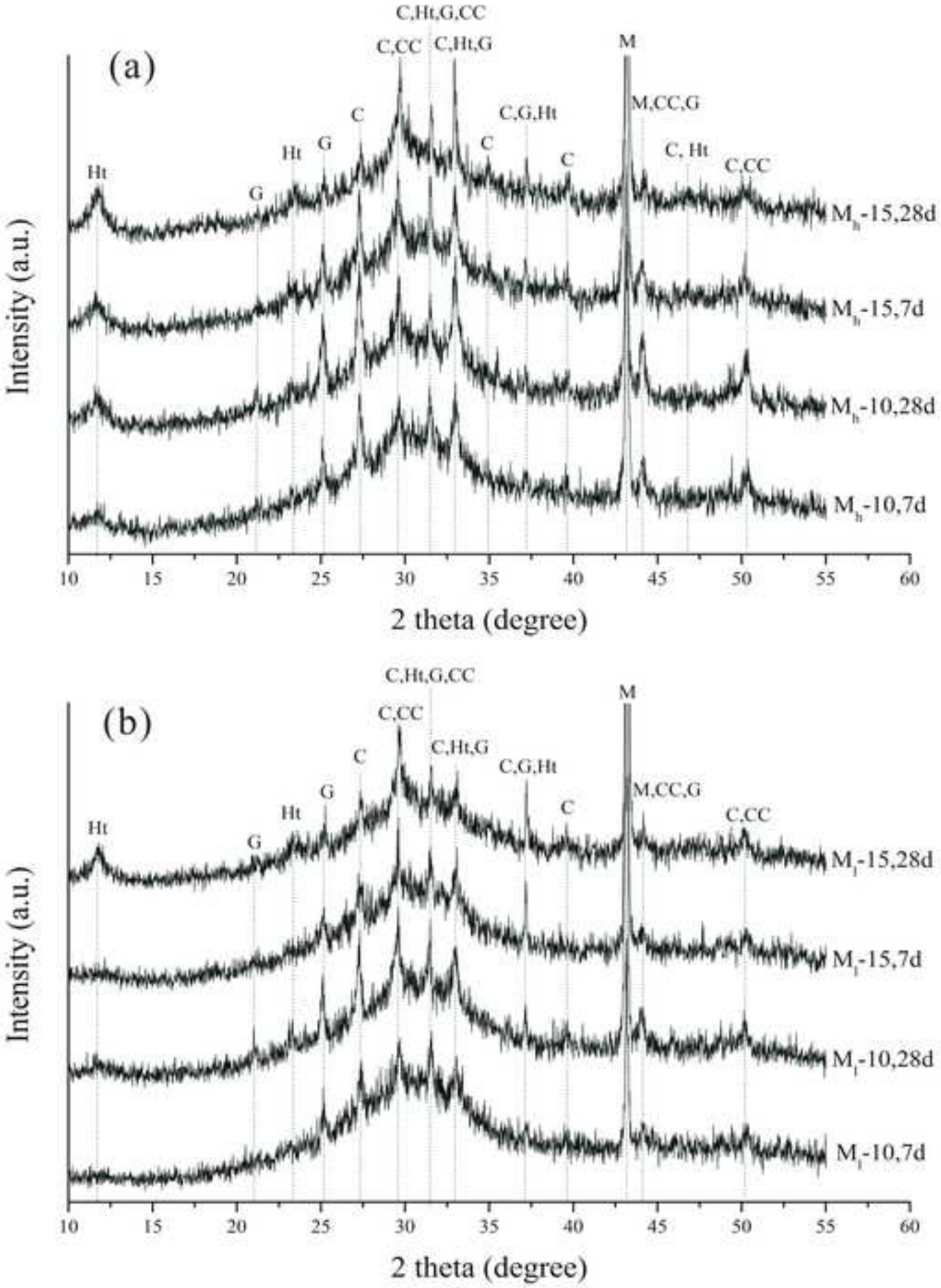

Figure
Click here to download high resolution image

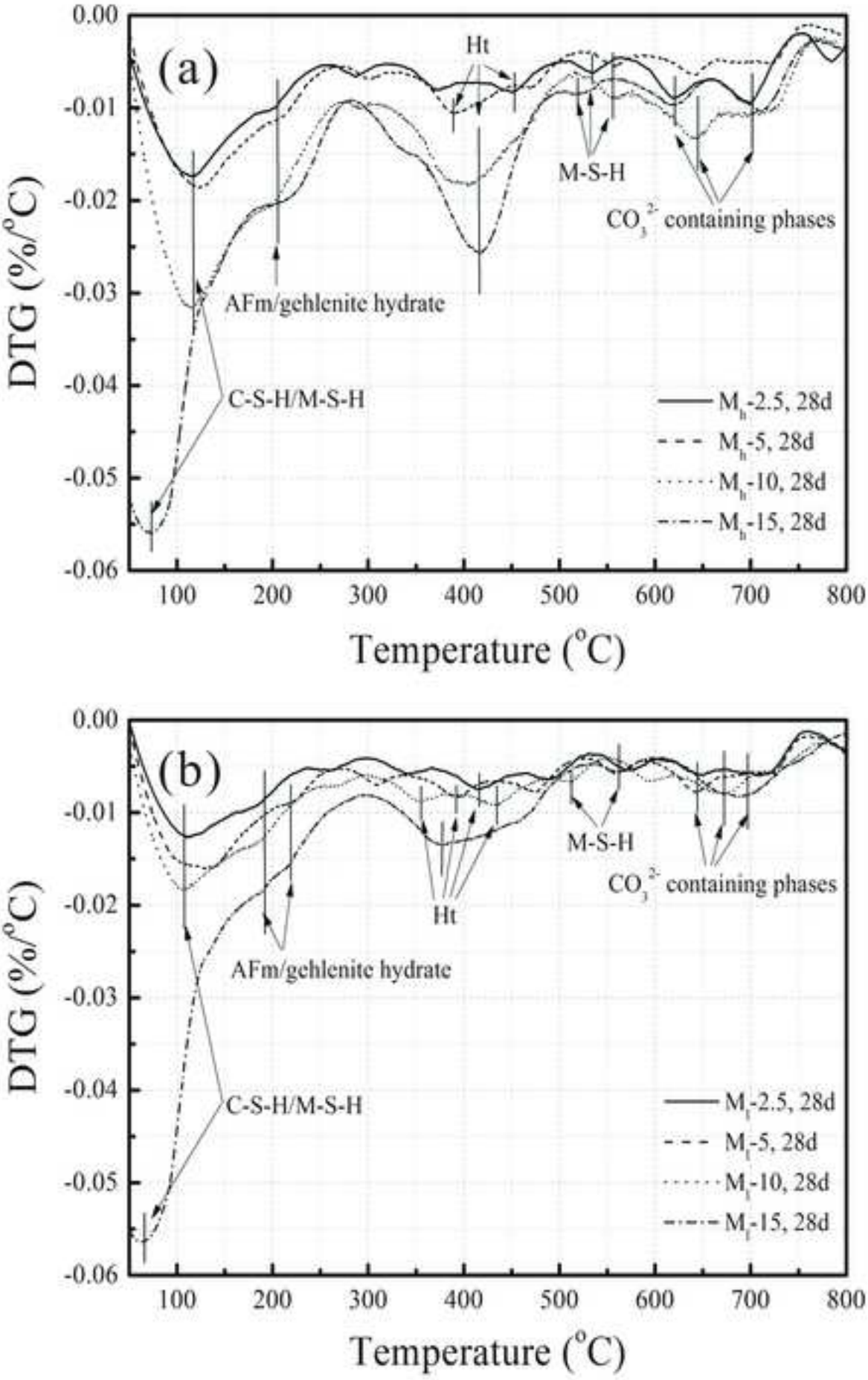

Figure
Click here to download high resolution image

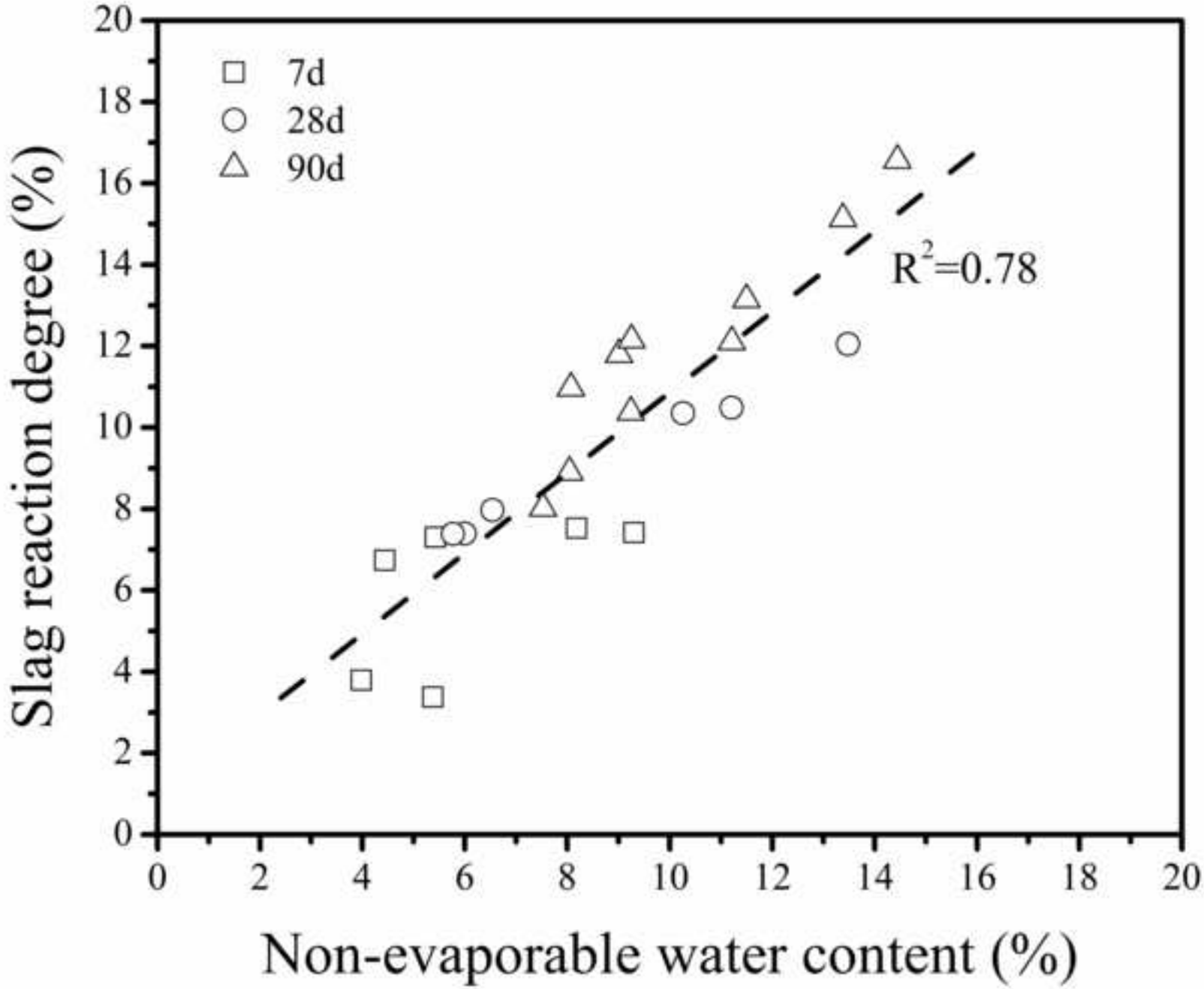

Figure
Click here to download high resolution image

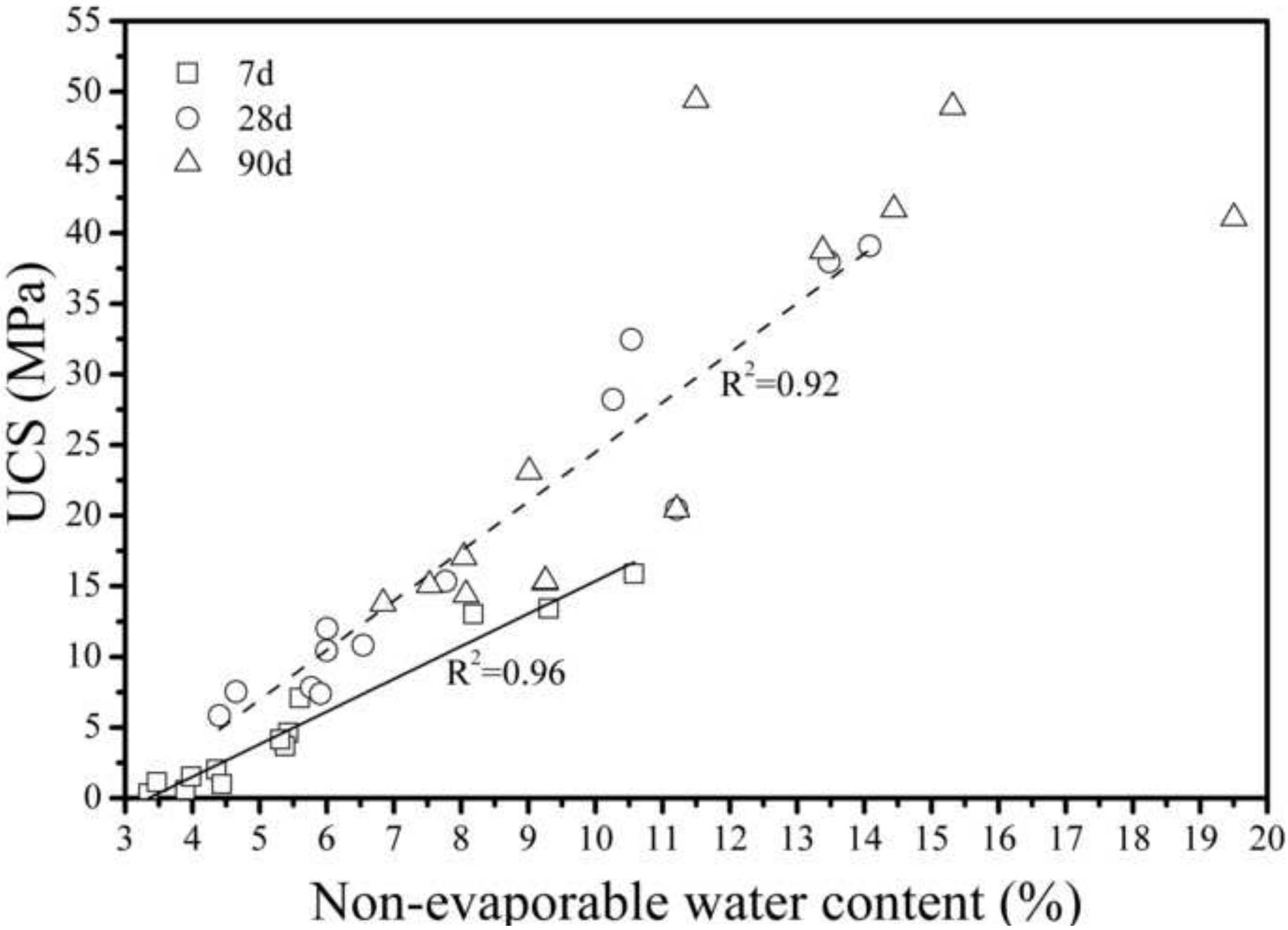

Figure

Click here to download high resolution image

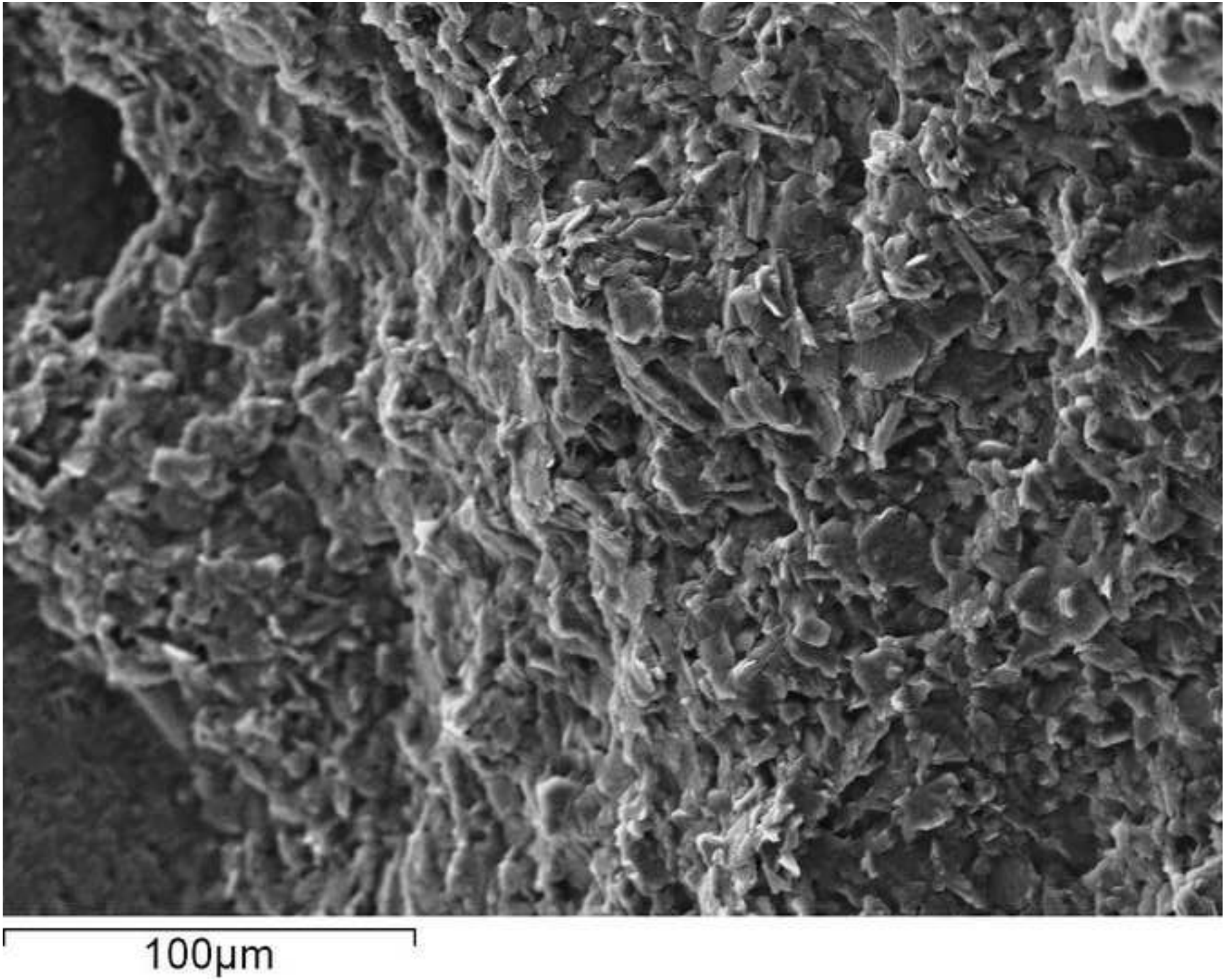

Figure

Click here to download high resolution image

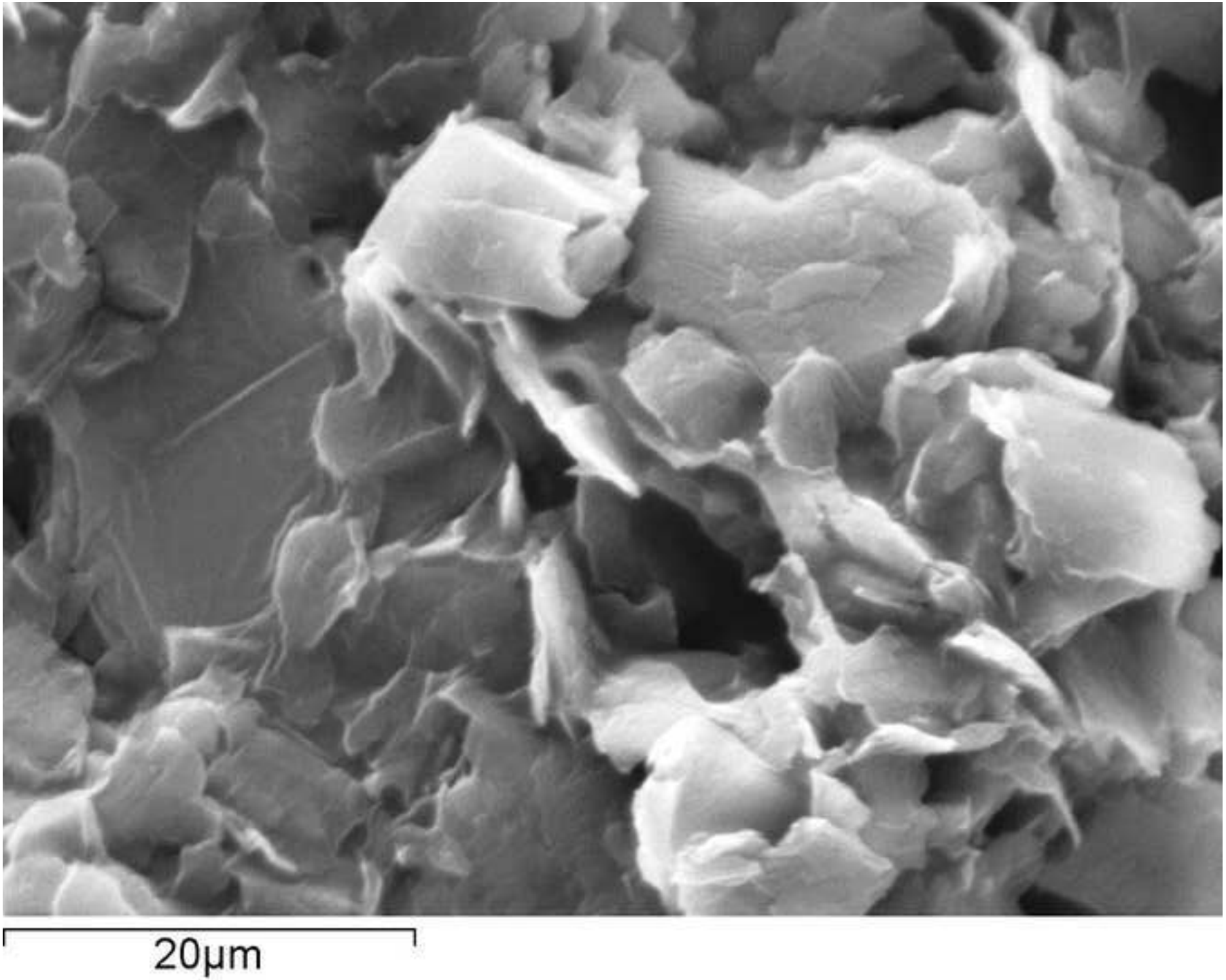

Figure

Click here to download high resolution image

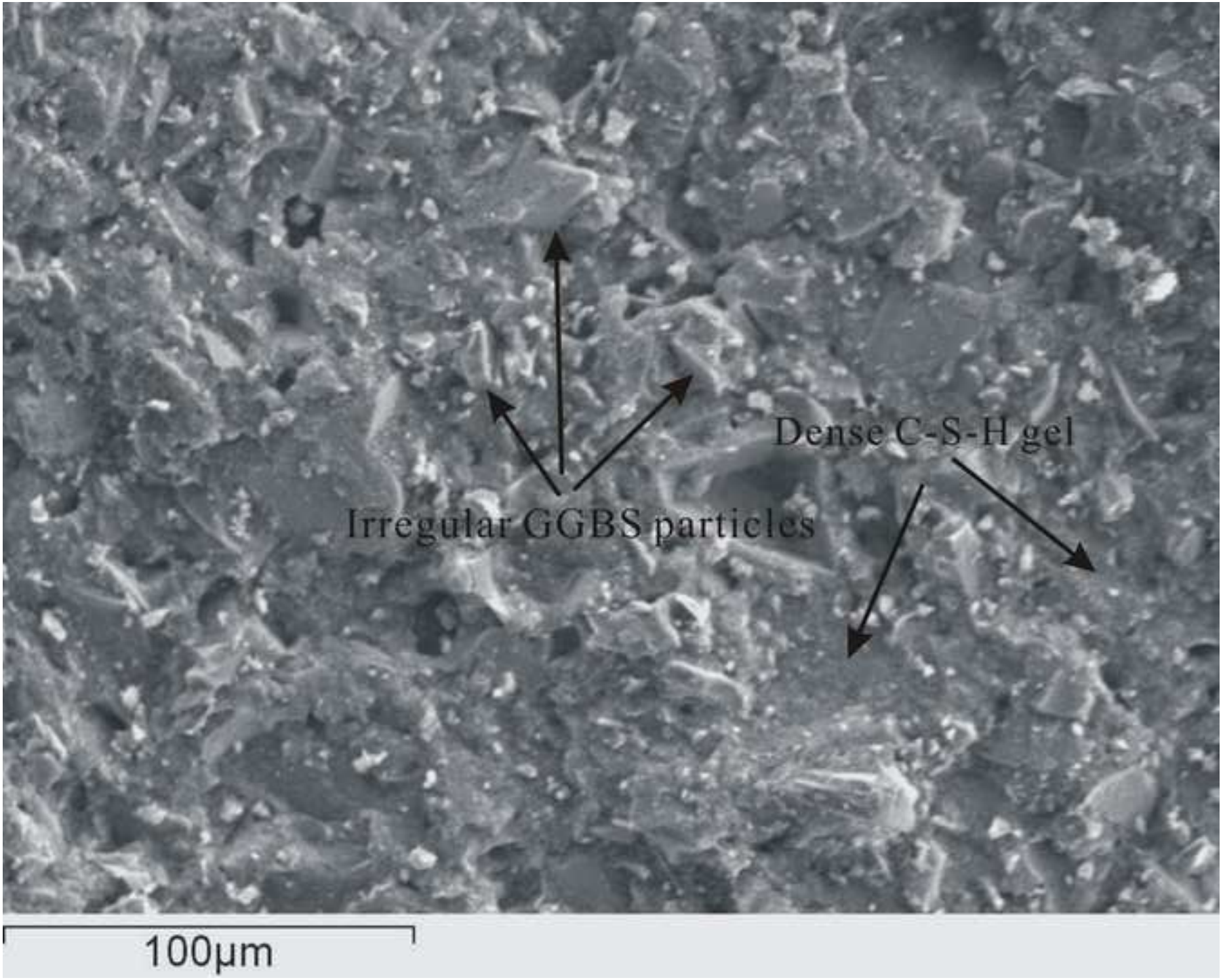

Figure

Click here to download high resolution image

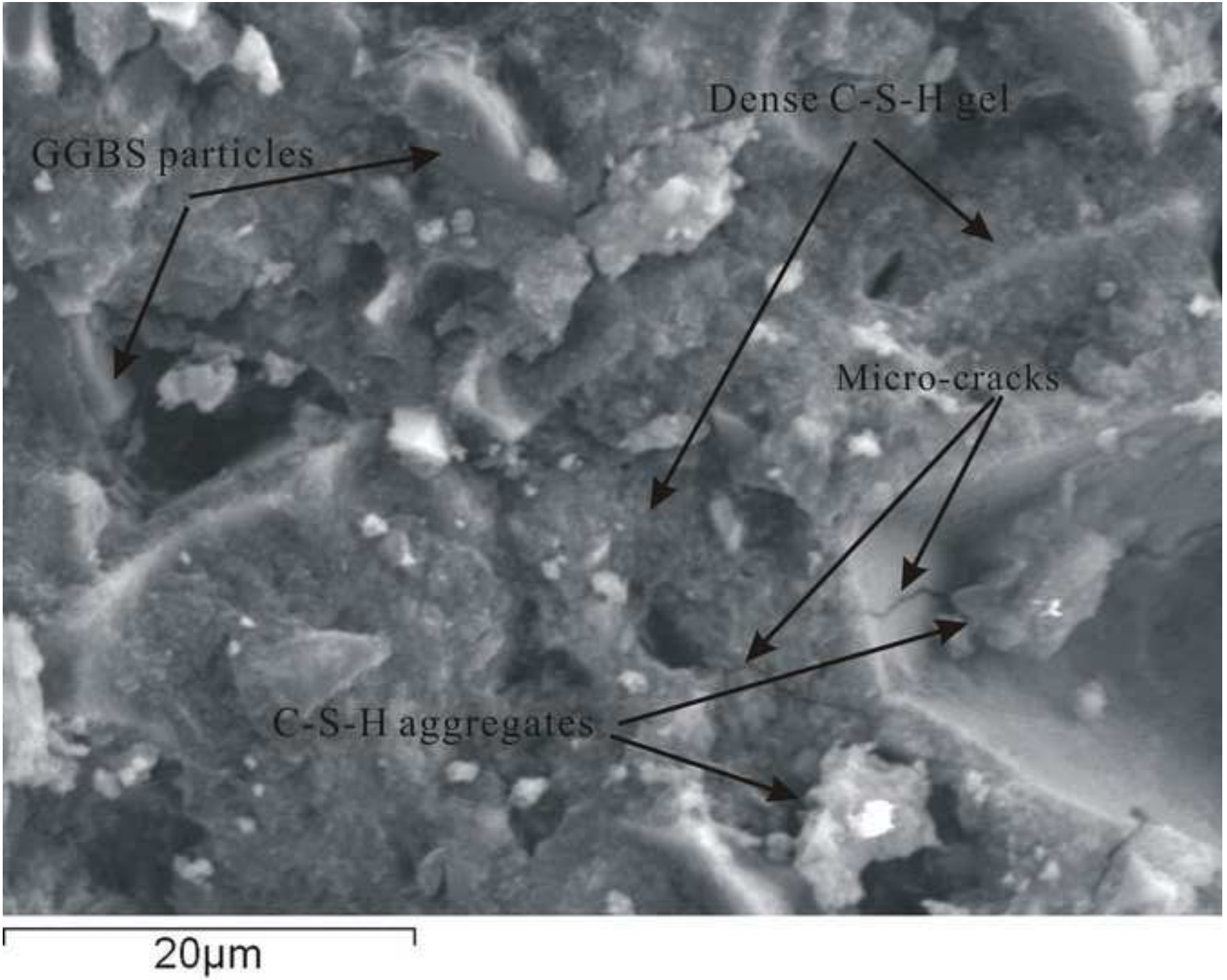

Figure

Click here to download high resolution image

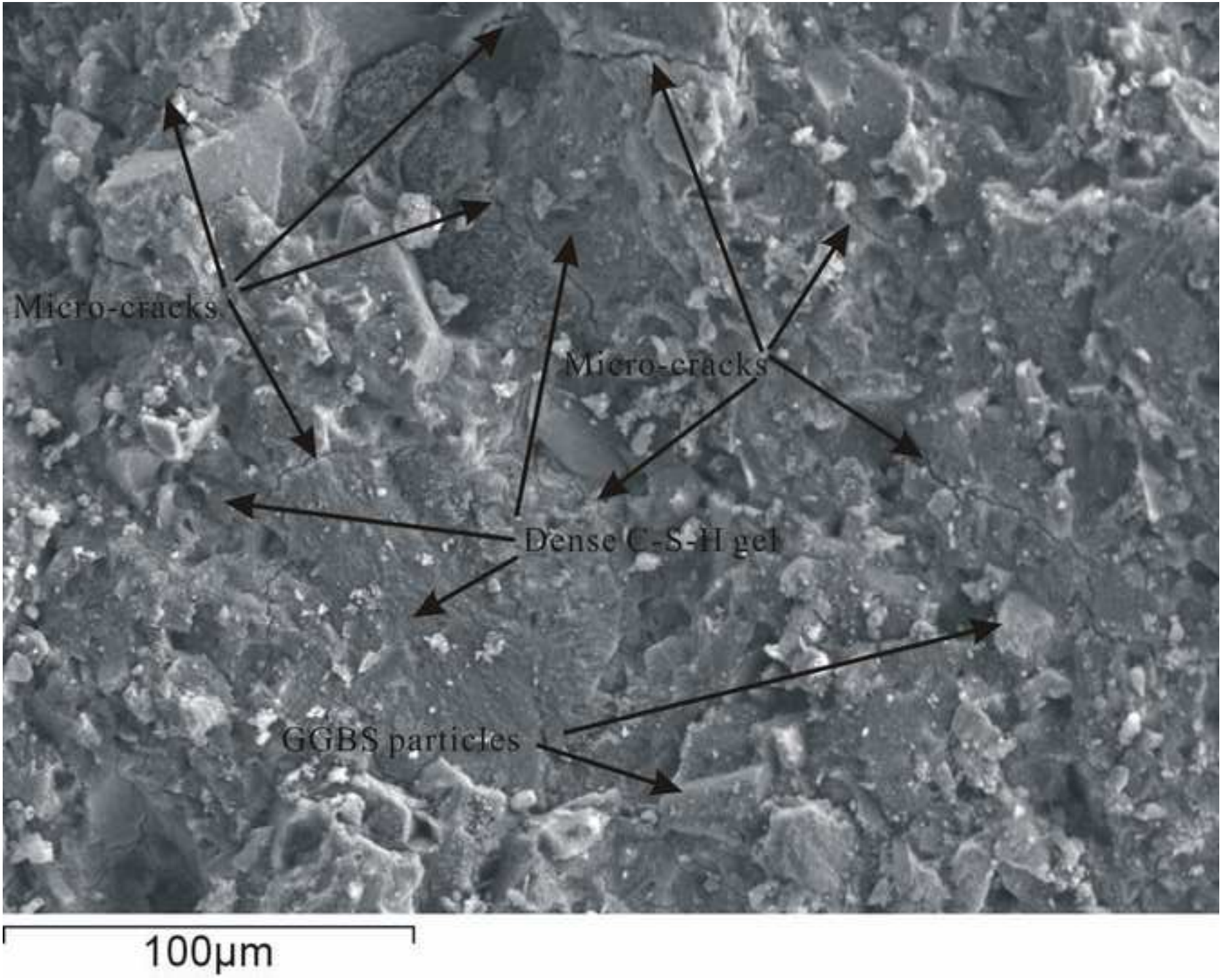

Figure

Click here to download high resolution image

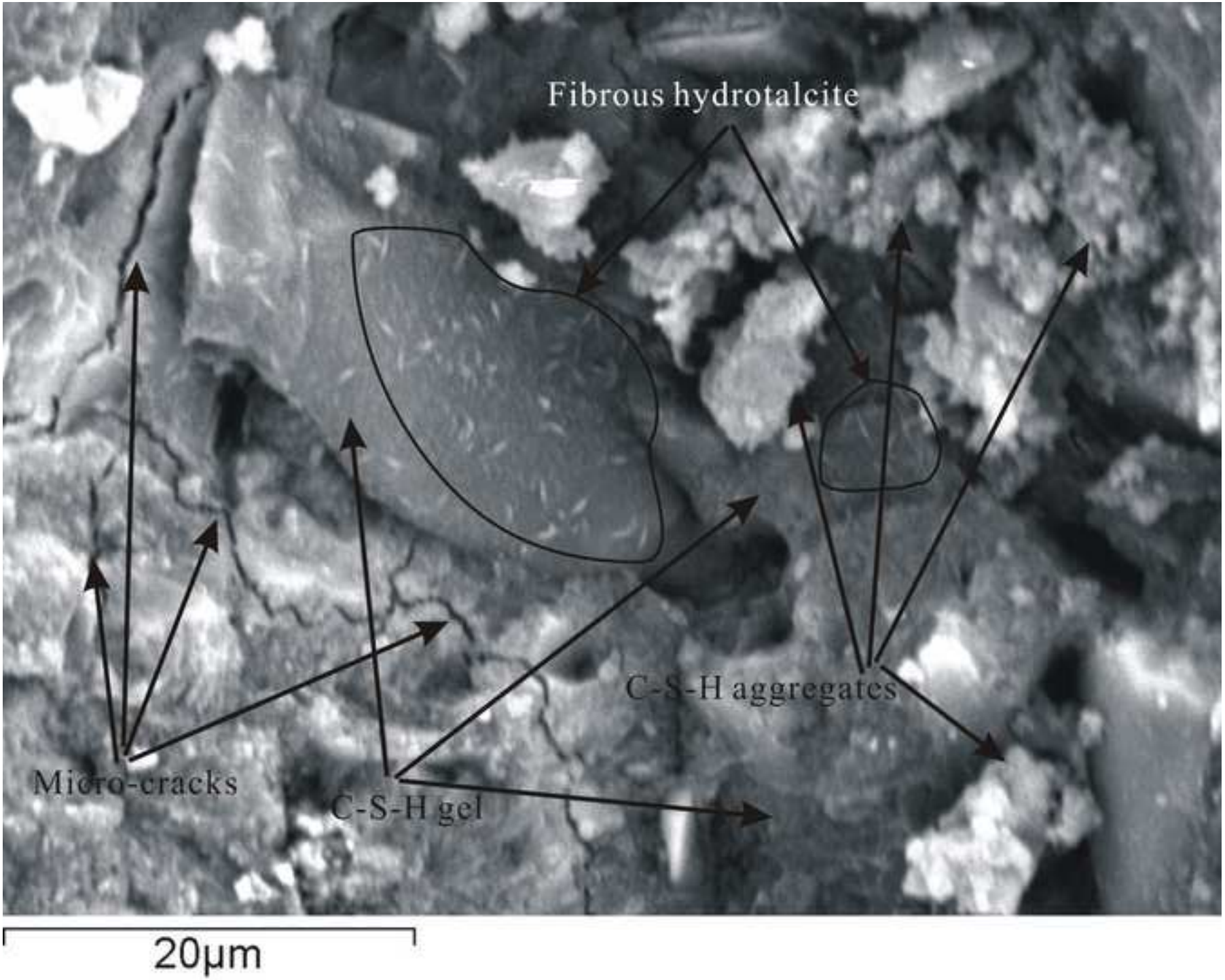

Figure

Click here to download high resolution image

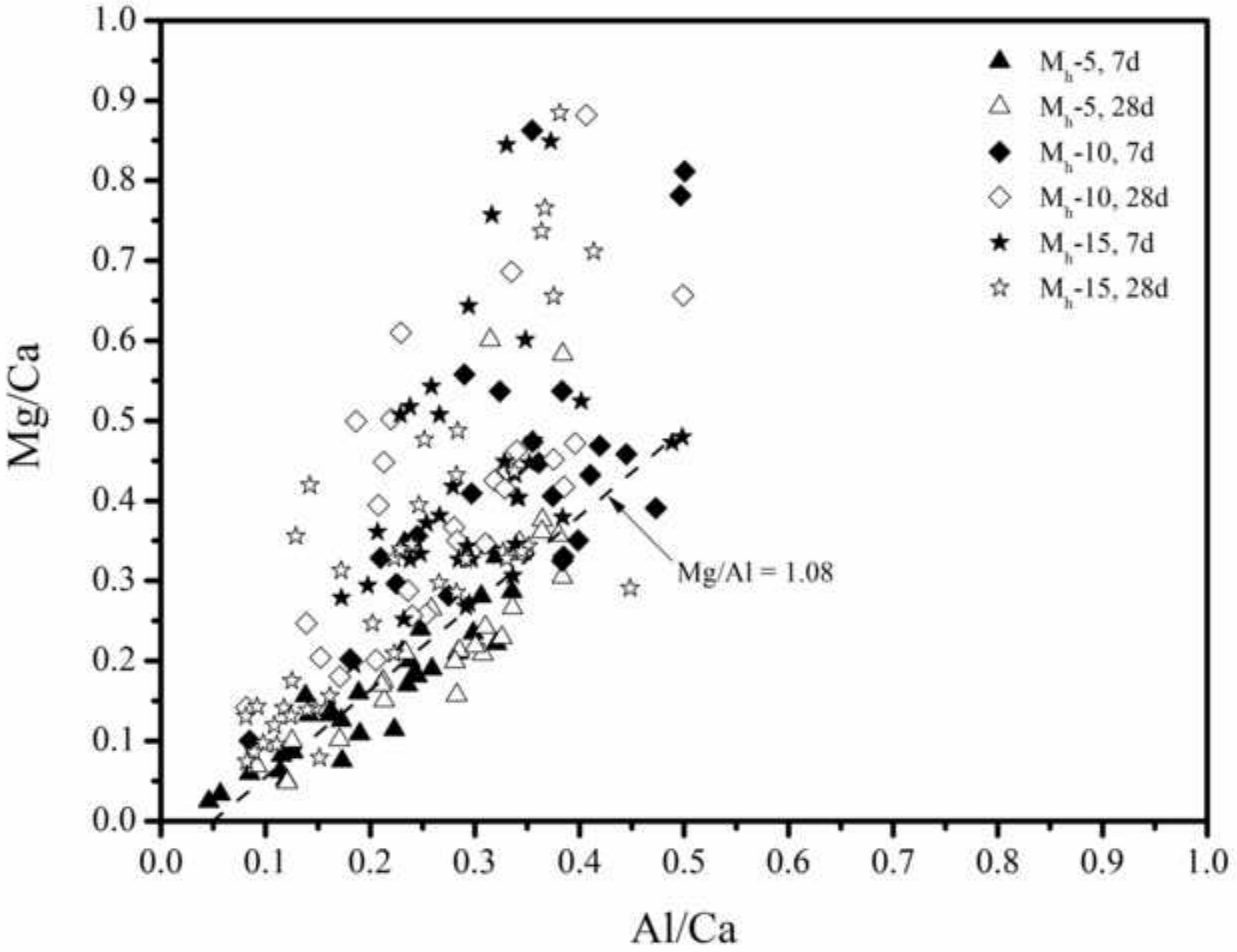

Figure 1 UCS development with time (a) M_h-GGBS blends (b) M_l-GGBS blends

Figure 2 Variation of pH with curing time (a) M_h-GGBS blends (b) M_l-GGBS blends

Figure 3 Slag reaction degrees with different MgO content

Figure 4 Effect of W/C on the strength of M_h-GGBS and C-10 blends

Figure 5 XRD patterns for (a) M_h-10 and M_h-15 and (b) M_l-10 and M_l-15 blends cured for 7 and 28days. Ht: hydrotalcite-like phases; C: tobermorite-like C-S-H; G: gelenite hydrate; CC: calcite; M: MgO

Figure 6 DTG curves for (a) M_h-GGBS blends and (b) M_l-GGBS blends cured for 28days

Figure 7 Relationship between slag reaction degree and NEW

Figure 8 Relationship between UCS of MgO-GGBS blends and NEW

Figure 9 SEM pictures for M_h-GGBS blends at 28 days (a)(b) 5% MgO; (c)(d) 10% MgO; (e)(f) 15% MgO

Figure 10 Mg/Ca against Al/Ca atom ratio plot for M_h-GGBS blends